Aggregate-selective removal of pathological tau via clustering-activated degraders

Jonathan Benn, Shi Cheng, Sophie Keeling, Annabel Smith, Marina Vaysburd, Dorothea Böken, Lauren Miller, Taxiarchis Katsinelos, Catarina Franco, Elian Dupré, et al.

▶ **To cite this version:**

Jonathan Benn, Shi Cheng, Sophie Keeling, Annabel Smith, Marina Vaysburd, et al.. Aggregate-selective removal of pathological tau via clustering-activated degraders. Science, 2024, 385 (6712), pp.1009-1016. ⟨10.1126/science.adp5186⟩. ⟨hal-04745023⟩

HAL Id: hal-04745023

https://hal.science/hal-04745023v1

Submitted on 19 Oct 2024

HAL is a multi-disciplinary open access archive for the deposit and dissemination of scientific research documents, whether they are published or not. The documents may come from teaching and research institutions in France or abroad, or from public or private research centers.

L'archive ouverte pluridisciplinaire **HAL**, est destinée au dépôt et à la diffusion de documents scientifiques de niveau recherche, publiés ou non, émanant des établissements d'enseignement et de recherche français ou étrangers, des laboratoires publics ou privés.

HAL Authorization

Title: Aggregate-selective removal of pathological tau via clustering-activated degraders

Authors: Jonathan Benn*[1†], Shi Cheng*[1†], Sophie Keeling[1], Annabel E Smith[1], Marina J Vaysburd[2], Dorothea Böken[1], Lauren VC Miller[2], Taxiarchis Katsinelos[1,2], Catarina Franco[2], Elian Dupré[3,4], Clément Danis[3,4,5], Isabelle Landrieu[3,4], Luc Buée[5], David Klenerman[1], Leo C James*[2,] William A McEwan*[1]

[1] UK Dementia Research Institute at the University of Cambridge, Hills Road, Cambridge, CB2 0AH, UK.

[2] MRC Laboratory of Molecular Biology, Cambridge CB2 0QH, UK.

[3] CNRS EMR9002 – BSI - Integrative Structural Biology, LabEx DISTALZ, F-59000 Lille, France.

[4] Univ. Lille, Inserm, CHU Lille, Institut Pasteur de Lille, U1167 - RID-AGE - Risk Factors and Molecular Determinants of Aging-Related Diseases, F-59000 Lille, France.

[5] Université Lille, Inserm, CHU Lille, Lille Neuroscience & Cognition, LabEx DISTALZ, F-59000 Lille, France.

*Corresponding author. J.B: jb2310@cam.ac.uk. S.C: chengshi1013@163.com. L.J: lcj@mrc-lmb.cam.ac.uk. W.M: wm305@cam.ac.uk.

[†]These authors contributed equally to this work.

Abstract: Homotypic protein assembly is a critical mediator of biological function and disease state. Selective degradation of protein assemblies, while sparing monomeric forms, is required for interrogation of biological mechanisms and assembly-specific therapeutic intervention. We have exploited the requirement of intermolecular clustering for activation of the E3 ligase TRIM21 to produce TRIM21-nanobody fusions capable of rapidly and selectively degrading assembled proteins. We demonstrate this approach against histone 2B-GFP and tau, a protein that undergoes pathological aggregation in Alzheimer's and other neurodegenerative diseases. Intracellular expression of TRIM21-nanobody degraders prevented or reversed tau aggregation in culture systems and in vivo, with minimal impact on soluble tau. Our results demonstrate that homotypic quaternary structure is a property of proteins that may be exploited for their selective degradation.

One-Sentence Summary: Redirecting a cytosolic immune pathway enables potent and aggregate-selective removal of pathological tau protein in cell and animal models.

Main Text

Introduction

The transition of soluble physiological proteins into pathological homotypic aggregates underlies many common neurodegenerative diseases. Tau is one such protein, whose aggregation correlates with symptomatic progression in Alzheimer's disease (*1*, *2*) and is therefore a target of therapeutic interest. Antisense oligonucleotides (ASOs) can reduce tau protein levels, ameliorating tau pathology in mice (*3*), and have now entered human trials (*4*, *5*). However, such nucleic acid approaches rely on reducing total protein pools and so loss of physiological protein is an unavoidable corollary. Toxicity is therefore anticipated, especially for targets where the physiological protein plays critical cellular roles. Methods that potently and selectively deplete aggregated proteins are therefore required.

The cytosolic antibody receptor and E3 ubiquitin ligase TRIM21 can mediate the destruction of antibody-bound targets including viruses (*6*), cellular proteins (*7*) and tau aggregates (*8*). This E3 ligase activity is induced via the clustering and cross-activation of TRIM21's RING domains (*9*, *10*), which is satisfied upon TRIM21 binding to polyvalent antibody-coated complexes (*11*) (Fig. 1A and B), resulting in destruction of the entire complex via the unfoldase p97/VCP and the proteasome (*12*, *13*)**.** However, the applicability of targeted protein degradation via this pathway is limited by the general inability of antibodies to access the intracellular domain. For instance, anti-tau immunotherapy can be dependent on TRIM21, but relies on extracellular "seed competent" tau aggregates importing antibodies into the cytosol where they engage and activate TRIM21 to neutralise the bound aggregates (*14*).

In this study we sought to exploit the clustering-dependent activation of TRIM21 to develop genetically encoded degraders that are activated in the context of assembled, but not monomeric, targets (Fig. 1C and D). By fusing the RING domain of TRIM21 to a target-specific nanobody we generated RING-nanobody (R-Nb) degraders that can be expressed in the nucelocytoplasm. Using tau as a substrate, R-Nb constructs were demonstrated to inhibit seeded tau aggregation and degrade pre-existing insoluble aggregates. Meanwhile, soluble tau was largely unaffected. R-Nb constructs therefore represent a new modality by which aggregated proteins may be selectively degraded, allowing for further interrogation of protein function and a potential route to the therapeutic removal of aggregated proteins implicated in neurodegenerative disease.

Tau targeted R-Nb rapidly degrades aggregated tau species

The repetitive nature of fibrillar tau aggregates was hypothesised to allow for the dense clustering of R-Nb degraders on their surface, inducing RING cross-activation and subsequent degradation. A variant of the anti-tau C-terminus nanobody F8-2, optimised for increased intracellular affinity (S54L+T127A), (*15*), was selected as a targeting domain (R-Nb$_{F8-2}$). This construct consisted of an N-terminal TRIM21 RING domain followed by the nanobody and a self-cleaving (T2A) mCherry reporter (Fig. S1A). To create a cell line model containing constitutively aggregated fluorescently tagged tau, HEK293 cells over-expressing soluble P301S tau-venus (*8*) (tau-venus soluble, TVS cells) were seeded with tau assemblies prepared from the brains of aged Tg2541 P301S tau transgenic mice (*16*) and clonally expanded (tau-venus aggregated, TVA cells). Immuno-gold electron microscopy confirmed the presence of fibrillar tau assemblies in TVA cells (Fig. S1B and C).

To assess the ability of R-Nb$_{F8-2}$ to degrade pre-formed tau-venus aggregates, TVA cells were modified to express R-Nb$_{F8-2}$, or controls, in a doxycycline (DOX) inducible manner. Addition of DOX resulted in engagement of tau aggregates by the nanobody and a rapid reduction of punctate tau-venus aggregates, concomitant with R-Nb$_{F8-2}$ and mCherry expression (Fig. 1E and F, Supp. Video 1, Fig S1D-F). 15 hours post-DOX addition, tau-venus appeared re-solubilised and microtubule-associated. TRIM21 RING or F8-2 alone did not substantially alter levels of tau-venus aggregates, despite comparable expression levels (Fig. S1D).

To probe the nature of tau-venus aggregates degraded by R-Nb$_{F8-2}$, the sarkosyl soluble and insoluble fractions from these cells following DOX treatment were examined. As expected, a reduction in insoluble total and phosphorylated (AT8, pSer202 & pThr205) tau was observed only in R-Nb$_{F8-2}$ expressing cells (Fig. 1G). Interestingly, biochemically soluble tau species were also partially reduced following R-Nb$_{F8-2}$ expression (Fig. 1H). Subsequent probing revealed that the depleted species ran as a distinct higher molecular weight band and were recognised by phospho-tau antibodies (Fig. 1I), therefore likely representing small hyperphosphorylated tau assemblies such as have previously been reported (*17*). Further interrogation of tau species remaining in TVA lysates was performed using single-molecule pull-down (SiMPull) super-resolution microscopy (*18*), revealing that tau assemblies of all sizes were reduced following R-Nb$_{F8-2}$ expression (+DOX) (Fig.1J and K).

Low affinity R-Nb constructs selectively degrade aggregated tau, including seed competent species

In its physiological state, tau exists as a soluble cytosolic or microtubule-bound protein. We hypothesised that recruitment of R-Nb degraders to soluble tau may not induce degradation due to the spatial separation of RING domains preventing cross-activation. As R-Nb recruitment density will also be driven by nanobody affinity, we further hypothesised this would determine aggregate selectivity. To test this, we assessed a panel of R-Nb constructs with a 1000-fold range of in vitro affinity for tau-venus. Variants of F8-2 were used alongside H3-2 (overlapping epitope with F8-2 (Fig. S2A and B)), with in vitro affinities (K_D) ranging from ~1.3 μM to 32 nM (*15*) (Fig. S2C and D). vhhGFP4, which targets venus with an affinity of 1 nM (*19*) was also used, with a nanobody (Nb139) against an irrelevant target (p53) being used as a negative control (*20*).

R-Nb constructs were transfected into TVA or TVS cells to assess their ability to degrade aggregated or soluble tau respectively. Super-resolution microscopy has confirmed that P301S tau-venus in TVS cells is localised to microtubules and free in the cytosol (*21*). All R-Nb constructs were soluble when expressed in HEK293 cells (Fig. S3A), and those capable of binding tau-venus elicited the degradation of aggregates in TVA cells (Fig. 2A). However, degradation of soluble tau-venus in TVS cells was only instigated by R-Nb constructs using high affinity nanobodies (Fig. 2B). All R-Nb constructs were expressed at similar levels (Fig. S3, B and C). Surprisingly, the degradation kinetics of tau-venus were not substantially affected by its aggregation state following expression of the R-Nb$_{vhhGFP4}$ degrader (Fig. S3 D-G). These results demonstrate that degradation may be driven by R-Nb clustering on the surface of fibrillar assemblies for low-affinity degraders, or by high affinity recruitment to more spatially separated targets, and that low affinity R-Nb constructs may permit aggregate-selective degradation. The R-Nb construct using F8-2$_{S54L+T127A}$ (used in Fig. 1) resulted in the highest level of aggregate degradation without affecting soluble tau and was therefore selected for use in subsequent experiments (referred to as R-Nb$_{F8-2}$).

To assess the selectivity of R-Nb$_{F8-2}$ degradation the proteome of TVA R-Nb$_{F8-2}$ cells +/- DOX was analysed via mass spectrometry, revealing that out of over 8,000 endogenous proteins quantified, only two (HMGCR and PNMA1) were moderately yet significantly (q-value = 0.01, fold change >2) affected following R-Nb$_{F8-2}$ expression (Fig. 2C). Interestingly overall levels of tau-venus protein were unaffected, again suggesting that R-Nb$_{F8-2}$ mediated degradation of aggregated tau is assembly state specific. To confirm that R-Nb$_{F8-2}$ does not degrade soluble tau, TVS cells were modified to express DOX inducible R-Nb$_{F8-2}$. 24 h after DOX addition cells expressed high levels of R-Nb$_{F8-2}$ (Fig. S4A), yet this had no effect on tau-venus protein levels (Fig. 2, D and E). Using this same cell line, we tested whether R-Nb$_{F8-2}$ expression would protect against seeded tau aggregation. TVS cells challenged with heparin-assembled P301S tau fibrils in the presence of Lipofectamine form quantifiable aggregated tau-venus puncta in a dose responsive manner (*8*), which was almost entirely prevented in TVS cells expressing R-Nb$_{F8-2}$ (Fig. 2F). R-Nb$_{F8-2}$ expression therefore specifically degrades aggregated tau and confers resistance to seeded tau aggregation.

TRIM21 mediated degradation is reliant on the UPS with involvement of the unfoldase p97/VCP (*6*, *12*). To investigate whether degradation of aggregated tau in TVA cells via R-Nb$_{F8-2}$ is reliant on these same mechanisms, we inhibited the E1 ubiquitin activating enzyme (UAE) with TAK-243; the proteasome with MG132 (Fig. S4B); or VCP with NMS-873 (Fig S4C). Alternatively, bafilomycin was used to inhibit autophagy (Fig. S4D). Solvent only (DMSO) and the inhibitors had minimal effects on R-Nb$_{F8-2}$ expression (Fig. S4E), and DMSO itself did not affect R-Nb$_{F8-2}$ mediated degradation (Fig. S4F). Inhibition of E1, VCP, and the proteasome significantly impaired the ability of R-Nb$_{F8-2}$ to degrade aggregated tau-venus (Fig. 2G). In contrast bafilomycin had no effect, confirming that R-Nb$_{F8-2}$ mediated degradation of aggregated tau, similar to TRIM21, requires the UPS with involvement of VCP.

The degradation of aggregated tau via VCP and the proteasome has been reported to result in production of further seed competent tau species (*21*, *22*). Lysates and supernatants from TVA cells expressing R-Nb$_{F8-2}$ or controls were therefore introduced into TVS cells to induce seeded tau-venus aggregation, with results demonstrating that only R-Nb$_{F8-2}$ expression reduced levels of seed competent tau species (Fig. 2H and S4G). The degradation of aggregated tau via R-Nb$_{F8-2}$ thus reduces total levels of seed competent tau species rather than increasing them.

In vivo application of R-Nb for CNS targets

To investigate whether R-Nb constructs can degrade proteins in the brain, we targeted GFP-tagged histone 2B (H2B-GFP), an oligomeric substrate amenable to TRIM21 mediated degradation (*11*). AAV1/2 encoding a GFP-targeted degrader (R-Nb$_{vhhGFP4}$) with a self-cleaving T2A-mCherry reporter was produced, alongside TRIM21 RING and vhhGFP4 only controls. Expression of all constructs was driven by a universal CAG promoter. AAV1/2 was injected unilaterally into the hippocampus of transgenic H2B-GFP mice at two-months of age, and homogenates prepared 30 days later from injected and contralateral hippocampi. GFP ELISA revealed that injection of AAV1/2 encoding R-Nb$_{vhhGFP4}$ led to a reduction of H2B-GFP in injected vs contralateral hippocampi (Fig. 3A). To ascertain whether degradation can occur over a shorter time period, H2B-GFP levels were compared 10- and 30-days post AAV1/2 R-Nb$_{vhhGFP4}$ injection via GFP ELISA. This revealed that H2B-GFP degradation in injected vs contralateral hippocampi was similar at both time points, confirming the rapid nature of R-Nb mediated degradation (Fig. 3B). Fluorescence microscopy was also used to assess H2B-GFP levels 30 days post AAV1/2 injection. Imaging confirmed that construct expression was largely confined to the injected hemisphere and that only AAV1/2 R-Nb$_{vhhGFP4}$ was capable of reducing H2B-GFP levels (Fig. 3C and D). Thus, R-Nb constructs are amenable to AAV delivery and can be used to degrade oligomeric protein substrates in the CNS in vivo.

Reduction of tau pathology in the aged mouse brain and primary neurons via R-Nb$_{F8-2}$

We next asked whether the tau-targeted R-Nb$_{F8-2}$ degrader could be delivered via AAV to counter tau pathology in aged Tg2541 mice, which express human 0N4R P301S tau under the Thy1 promoter. AAV1/2 vectors bearing R-Nb$_{F8-2}$ under a CAG promoter were injected unilaterally into the frontal cortex of 5.5-month-old mice, at which point their brains exhibit substantial AT8-positive tau pathology (Fig. S5A). Examination of brains 30 (Fig. 4A) or 10 (Fig. S5B) days later via immunofluorescence (IF) revealed that R-Nb$_{F8-2}$ expression was largely restricted to the injected hemisphere, and that this was associated with a reduction in AT8 staining compared to the contralateral side. Only expression of R-Nb$_{F8-2}$, and not TRIM21 RING or F8-2 only controls, reduced levels of AT8 staining in the injected hemisphere (Fig. 4B). Frontal cortex hemispheres from mice treated with R-Nb$_{F8-2}$ AAV1/2 were homogenised and probed for phosphorylated (AT100, pThr212 & pSer214) and total tau protein, revealing that pTau levels were reduced in injected hemispheres compared to contralateral sides, but that total tau levels remained unaffected (Fig. 4C).

Encouraged by these results demonstrating a reduction of tau pathology in aged mice, the ability of R-Nb$_{F8-2}$ to prevent neuronal seeded tau aggregation was assessed using primary mouse neurons from neonatal Tg2541 mice. The addition of heparin assembled P301S tau fibrils to these cultures induced tau aggregation, visualised as pTau positive cell bodies and puncta via IF. Seeded aggregation was reduced by pre-treating neurons with AAV1/2 bearing R-Nb$_{F8-2}$ under the neuron specific hSyn promoter (Fig. 4D and E). This reduction was observed in both neuronal cell bodies and dendritic compartments (Fig S5C and D). Conversely, pre-treatment with TRIM21 RING or F8-2 only AAV1/2 had no effect on seeded tau aggregation (Fig. 4E), despite similar expression levels as R-Nb$_{F8-2}$ (Fig. S5E). Neither R-Nb$_{F8-2}$ expression nor the AAV1/2 vector itself affected cell viability (Fig. S5F). To test whether R-Nb$_{F8-2}$ expression reduced the formation of seed

competent tau aggregates in this context, lysates from tau-seeded neurons pre-treated with varying doses of R-Nb$_{F8-2}$ AAV1/2 were interrogated in TVS HEK cells, revealing that R-Nb$_{F8-2}$ expression reduced the formation of seed competent tau in a dose responsive manner (Fig 4F). To confirm that R-Nb$_{F8-2}$ mediated neutralisation of seeded tau aggregation is dependent on its E3 ligase catalytic activity, two RING-inactivating mutations (M72E and I18R) (*23*) were introduced into the R-Nb$_{F8-2}$ construct. Pretreatment of neurons with AAV1/2 encoding this catalytically dead R-Nb$_{F8-2}$ did not reduce seeded tau aggregation compared to untransduced controls (Fig 4G), despite expression being similar to the active R-Nb$_{F8-2}$ construct (Fig. S5G).

The ability of R-Nb$_{F8-2}$ to reduce tau pathology in aged mice only days after AAV1/2 administration suggests that pre-existing neuronal tau aggregates are being degraded. To examine this possibility, primary mouse neurons expressing P301S tau-venus were treated with heparin assembled P301S tau aggregates and imaged longitudinally in situ. Seeded aggregates were detectable as bright venus puncta which, post-fixation, co-localised with AT8 staining (Fig. S5H). Remarkably, addition of R-Nb$_{F8-2}$ AAV1/2 caused large tau-venus aggregates to be rapidly cleared following R-Nb$_{F8-2}$ expression (Fig. 4H and Supp. Video 2). These results demonstrate that R-Nb$_{F8-2}$ expression can prevent and reverse tau aggregation in neurons, and can rapidly reduce tau pathology in an aged mouse model of tauopathy.

Global CNS expression of R-Nb$_{F8-2}$ reduces tau pathology in mice

To be effective in clinical applications, broad transduction of the brain would likely be required to express R-Nb degraders in a majority of cells affected by tau pathology. In mice, this may be achieved through the use of engineered AAV capsids such as AAV$_{9P31}$, a variant capable of transducing the brain following peripheral intravenous administration (*24*) (Fig. S6A). To determine the feasibility of this approach, R-Nb$_{F8-2}$ was packaged into AAV$_{9P31}$ under the hSyn promoter and delivered as a single tail vein dose to Tg2541 mice in either a short (10-day) or long (2-month) experimental protocol (Fig. 5A). In the 10-day protocol, R-Nb$_{F8-2}$ AAV$_{9P31}$ was administered to 5.5-month-old (Day 166) mice, with tau pathology assessed 10 days later via IF and western blot. AT8 staining of the frontal cortex revealed that R-Nb$_{F8-2}$ AAV$_{9P31}$ administration led to a decrease in pTau pathology compared to untreated mice (Fig. 5B and C). Tg2541 mice also develop severe spinal cord tau pathology by 5.5 months (*25*), which was reduced in individuals treated with R-Nb$_{F8-2}$ AAV$_{9P31}$ (Fig. 5D and E). Immunoblotting of whole brain lysates (Fig. S6B) revealed decreased levels of pTau in mice treated with R-Nb$_{F8-2}$ AAV$_{9P31}$ (Fig. S6C), whilst total tau levels remained unaffected (Fig. S6D). Similar results were obtained from spinal cord lysates (Fig. S6E, F and G).

Under the two-month treatment protocol, four-month-old mice (Day 123) were injected with R-Nb$_{F8-2}$ AAV$_{9P31}$, with sarkosyl soluble and insoluble fractions prepared from whole brain lysates two months later (Day 182). Insoluble tau phosphorylated at Ser396 (Fig. S6H), Ser422 and Ser202&Thr205 (AT8) was substantially reduced in R-Nb$_{F8-2}$ AAV$_{9P31}$ treated mice compared to untreated controls (Fig. 5F). Insoluble total tau running at the same weight as these phosphorylated species was also depleted in samples from treated mice. Unexpectedly, soluble total tau was somewhat reduced in R-Nb$_{F8-2}$ AAV$_{9P31}$ treated mice, which may be due to unoptimized dosing in this longer treatment protocol. As previous, the delivery of brain lysates to TVS cells revealed that R-Nb$_{F8-2}$ AAV$_{9P31}$ treatment reduced levels of seed competent tau species in the brain compared

to untreated mice (Fig 5G). These results demonstrate that the R-Nb strategy can be used to reduce protein aggregates rapidly and durably at scale in the mammalian brain.

Discussion

By fusing the E3 catalytic RING domain of TRIM21 to a target specific nanobody, we have engineered conditionally active degraders (R-Nb) that selectively degrade homotypic protein assemblies. R-Nb constructs using a tau specific nanobody were capable of rapidly clearing intracellular hyperphosphorylated and seed competent tau aggregates in various in vitro and in vivo models, whilst leaving native soluble tau largely unaffected. Degradation of a second substrate, histone 2B-GFP, demonstrates that the R-Nb approach can also achieve targeted protein degradation in the nucleus.

Fibrillar aggregates have long been considered challenging substrates for cellular degradation machinery. Previous studies have demonstrated that degradation by chaperones and the proteasome can produce an increased number of smaller aggregates, potentially mobilising seed competent species (*22*, *26*). We show here however that R-Nb degraders can successfully remove pre-formed insoluble tau aggregates, leading to a net decrease in seed-competent species. We speculate that the established role of TRIM21 in the destruction of cytosolic antibody-bound viruses in a time-sensitive manner likely renders it especially suited to be co-opted for this task.

The ability of R-Nb constructs to specifically target and deplete homotypic protein assemblies may aid in deconvoluting the contribution of assembled protein species towards neurodegenerative processes. Further studies assessing the phenotypic consequences of R-Nb mediated aggregate depletion are required for assessing aggregate-selective degraders as a therapeutic modality. If realised, this approach offers two key advantages over current strategies. First, unlike other interventions such as immunotherapy, these degraders are not reliant on intercepting extracellular tau assemblies, but are expressed within neurons to remove existing aggregates and prevent further aggregation. It would therefore be expected to operate irrespective of whether aggregation occurred via seeding or through cell-autonomous mechanisms. Second, the monomer sparing quality of the approach offers a method by which the cellular functions of tau could be preserved, while pathological assemblies are removed. ASO studies suggest that tau depletion in the brain is well tolerated in phase I trials (*4*, *5*). However, animal studies find phenotypes associated with total tau depletion, raising unknowns surrounding the effect of chronic depletion (*27*)**.** Further studies exploring the functional consequences of aggregate-selective versus total tau depletion, alongside long-term toxicity profiling, will inform the feasibility of R-Nb constructs as a therapeutic modality against tau and other aggregating proteins in neurodegenerative diseases.

References

1. P. T. Nelson, I. Alafuzoff, E. H. Bigio, C. Bouras, H. Braak, N. J. Cairns, R. J. Castellani, B. J. Crain, P. Davies, K. Del Tredici, C. Duyckaerts, M. P. Frosch, V. Haroutunian, P. R. Hof, C. M. Hulette, B. T. Hyman, T. Iwatsubo, K. A. Jellinger, G. A. Jicha, E. Kövari, W. A. Kukull, J. B. Leverenz, S. Love, I. R. MacKenzie, D. M. Mann, E. Masliah, A. C. McKee, T. J. Montine, J. C. Morris, J. A. Schneider, J. A. Sonnen, D. R. Thal, J. Q. Trojanowski, J. C. Troncoso, T. Wisniewski, R. L. Woltjer, T. G. Beach, Correlation of Alzheimer Disease Neuropathologic Changes With Cognitive Status: A Review of the Literature. *J Neuropathol Exp Neurol* **71**, 362–381 (2012).
2. B. Hanseeuw, H. I. L. Jacobs, A. Becker, R. F. Buckley, M. J. Properzi, M. E. Farrell, A. P. Schultz, J. S. Sanchez, J. P. Chhatwal, J. C. Price, R. A. Sperling, K. A. Johnson, Longitudinal associations between amyloid and tau-PET: Impact for prevention trials. *Alzheimer's & Dementia* **17** (2021).
3. S. L. DeVos, R. L. Miller, K. M. Schoch, B. B. Holmes, C. S. Kebodeaux, A. J. Wegener, G. Chen, T. Shen, H. Tran, B. Nichols, T. A. Zanardi, H. B. Kordasiewicz, E. E. Swayze, C. F. Bennett, M. I. Diamond, T. M. Miller, Tau Reduction Prevents Neuronal Loss and Reverses Pathological Tau Deposition and Seeding in Mice with Tauopathy. *Sci Transl Med* **9** (2017).
4. A. L. Edwards, J. A. Collins, C. Junge, H. Kordasiewicz, L. Mignon, S. Wu, Y. Li, L. Lin, J. DuBois, R. M. Hutchison, N. Ziogas, M. Shulman, L. Martarello, D. Graham, R. Lane, S. Budd Haeberlein, J. Beaver, Exploratory Tau Biomarker Results From a Multiple Ascending-Dose Study of BIIB080 in Alzheimer Disease. *JAMA Neurol* **80**, 1344 (2023).
5. C. J. Mummery, A. Börjesson-Hanson, D. J. Blackburn, E. G. B. Vijverberg, P. P. De Deyn, S. Ducharme, M. Jonsson, A. Schneider, J. O. Rinne, A. C. Ludolph, R. Bodenschatz, H. Kordasiewicz, E. E. Swayze, B. Fitzsimmons, L. Mignon, K. M. Moore, C. Yun, T. Baumann, D. Li, D. A. Norris, R. Crean, D. L. Graham, E. Huang, E. Ratti, C. F. Bennett, C. Junge, R. M. Lane, Tau-targeting antisense oligonucleotide MAPTRx in mild Alzheimer's disease: a phase 1b, randomized, placebo-controlled trial. *Nature Medicine 2023 29:6* **29**, 1437–1447 (2023).
6. D. L. Mallery, W. A. McEwan, S. R. Bidgood, G. J. Towers, C. M. Johnson, L. C. James, Antibodies mediate intracellular immunity through tripartite motif-containing 21 (TRIM21). *Proc Natl Acad Sci U S A* **107**, 19985–19990 (2010).
7. D. Clift, C. So, W. A. McEwan, L. C. James, M. Schuh, Acute and rapid degradation of endogenous proteins by Trim-Away. *Nature Protocols 2018 13:10* **13**, 2149–2175 (2018).
8. W. A. McEwan, B. Falcon, M. Vaysburd, D. Clift, A. L. Oblak, B. Ghetti, M. Goedert, L. C. James, Cytosolic Fc receptor TRIM21 inhibits seeded tau aggregation. *Proc Natl Acad Sci U S A* **114**, 574–579 (2017).
9. L. Kiss, D. Clift, N. Renner, D. Neuhaus, L. C. James, RING domains act as both substrate and enzyme in a catalytic arrangement to drive self-anchored ubiquitination. *Nature Communications 2021 12:1* **12**, 1–12 (2021).
10. L. Kiss, J. Zeng, C. F. Dickson, D. L. Mallery, J. C. Yang, S. H. McLaughlin, A. Boland, D. Neuhaus, L. C. James, A tri-ionic anchor mechanism drives Ube2N-specific recruitment and K63-chain ubiquitination in TRIM ligases. *Nature Communications 2019 10:1* **10**, 1–13 (2019).
11. J. Zeng, A. F. Santos, A. S. Mukadam, M. Osswald, D. A. Jacques, C. F. Dickson, S. H. McLaughlin, C. M. Johnson, L. Kiss, J. Luptak, N. Renner, M. Vaysburd, W. A. McEwan, E. Morais-de-Sá, D. Clift, L. C. James, Target-induced clustering activates Trim-Away of pathogens and proteins. *Nature Structural & Molecular Biology 2021 28:3* **28**, 278–289 (2021).
12. F. Hauler, D. L. Mallery, W. A. McEwan, S. R. Bidgood, L. C. James, AAA ATPase p97/VCP is essential for TRIM21-mediated virus neutralization. *Proceedings of the National Academy of Sciences* **109**, 19733–19738 (2012).
13. A. J. Fletcher, D. L. Mallery, R. E. Watkinson, C. F. Dickson, L. C. James, J. Luban, Sequential ubiquitination and deubiquitination enzymes synchronize the dual sensor and effector functions of TRIM21. *Proc Natl Acad Sci U S A* **112**, 10014–10019 (2015).
14. A. S. Mukadam, L. V. C. Miller, A. E. Smith, M. Vaysburd, S. A. Sakya, S. Sanford, S. Keeling, B. J. Tuck, T. Katsinelos, C. Green, L. Skov, S. S. Kaalund, S. Foss, K. Mayes, K. O'Connell, M. Wing, C. Knox, J. Banbury, E. Avezov, J. B. Rowe, M. Goedert, J. T. Andersen, L. C. James, W. A. McEwan, Cytosolic antibody receptor TRIM21 is required for effective tau immunotherapy in mouse models. *Science (1979)* **379**, 1336–1341 (2023).

15. E. Dupré, C. Danis, A. Arrial, X. Hanoulle, M. Homa, F. X. Cantrelle, H. Merzougui, M. Colin, J. C. Rain, L. Buée, I. Landrieu, Single Domain Antibody Fragments as New Tools for the Detection of Neuronal Tau Protein in Cells and in Mice Studies. *ACS Chem Neurosci* **10**, 3997–4006 (2019).
16. B. Allen, E. Ingram, M. Takao, M. J. Smith, R. Jakes, K. Virdee, H. Yoshida, M. Holzer, M. Craxton, P. C. Emson, C. Atzori, A. Migheli, R. Anthony Crowther, B. Ghetti, M. G. Spillantini, M. Goedert, Abundant tau filaments and nonapoptotic neurodegeneration in transgenic mice expressing human P301S tau protein. *J Neurosci* **22**, 9340–9351 (2002).
17. B. Hyman, All the Tau We Cannot See. *Annu Rev Med* **74**, 503–514 (2023).
18. D. Böken, D. Cox, M. Burke, J. Y. L. Lam, T. Katsinelos, J. S. H. Danial, E. Fertan, W. A. McEwan, J. B. Rowe, D. Klenerman, Single-Molecule Characterization and Super-Resolution Imaging of Alzheimer's Disease-Relevant Tau Aggregates in Human Samples. *Angew Chem Int Ed Engl* **63**, e202317756 (2024).
19. M. H. Kubala, O. Kovtun, K. Alexandrov, B. M. Collins, Structural and thermodynamic analysis of the GFP:GFP-nanobody complex. *Protein Sci* **19**, 2389 (2010).
20. J. Bethuyne, S. De Gieter, O. Zwaenepoel, A. Garcia-Pino, K. Durinck, A. Verhelle, G. Hassanzadeh-Ghassabeh, F. Speleman, R. Loris, J. Gettemans, A nanobody modulates the p53 transcriptional program without perturbing its functional architecture. *Nucleic Acids Res* **42**, 12928 (2014).
21. E. Dimou, T. Katsinelos, G. Meisl, B. J. Tuck, S. Keeling, A. E. Smith, E. Hidari, J. Y. L. Lam, M. Burke, S. Lövestam, R. T. Ranasinghe, W. A. McEwan, D. Klenerman, Super-resolution imaging unveils the self-replication of tau aggregates upon seeding. *Cell Rep* **42**, 112725 (2023).
22. I. Saha, P. Yuste-Checa, M. Da Silva Padilha, Q. Guo, R. Körner, H. Holthusen, V. A. Trinkaus, I. Dudanova, R. Fernández-Busnadiego, W. Baumeister, D. W. Sanders, S. Gautam, M. I. Diamond, F. U. Hartl, M. S. Hipp, The AAA+ chaperone VCP disaggregates Tau fibrils and generates aggregate seeds in a cellular system. *Nature Communications 2023 14:1* **14**, 1–17 (2023).
23. L. Kiss, T. Rhinesmith, J. Luptak, C. F. Dickson, J. Weidenhausen, S. Smyly, J. C. Yang, S. L. Maslen, I. Sinning, D. Neuhaus, D. Clift, L. C. James, Trim-Away ubiquitinates and degrades lysine-less and N-terminally acetylated substrates. *Nature Communications 2023 14:1* **14**, 1–17 (2023).
24. M. Nonnenmacher, W. Wang, M. A. Child, X. Q. Ren, C. Huang, A. Z. Ren, J. Tocci, Q. Chen, K. Bittner, K. Tyson, N. Pande, C. H. Y. Chung, S. M. Paul, J. Hou, Rapid evolution of blood-brain-barrier-penetrating AAV capsids by RNA-driven biopanning. *Mol Ther Methods Clin Dev* **20**, 366–378 (2021).
25. J. A. Macdonald, I. F. Bronner, L. Drynan, J. Fan, A. Curry, G. Fraser, I. Lavenir, M. Goedert, Assembly of transgenic human P301S Tau is necessary for neurodegeneration in murine spinal cord. *Acta Neuropathol Commun* **7**, 44 (2019).
26. E. Nachman, A. S. Wentink, K. Madiona, L. Bousset, T. Katsinelos, K. Allinson, H. Kampinga, W. A. McEwan, T. R. Jahn, R. Melki, A. Mogk, B. Bukau, C. Nussbaum-Krammer, Disassembly of Tau fibrils by the human Hsp70 disaggregation machinery generates small seeding-competent species. *Journal of Biological Chemistry* **295**, 9676–9690 (2020).
27. S. A. Kent, T. L. Spires-Jones, C. S. Durrant, The physiological roles of tau and Aβ: implications for Alzheimer's disease pathology and therapeutics. *Acta Neuropathol* **140**, 417–447 (2020).
28. M. Goedert, M. G. Spillantini, R. Jakes, D. Rutherford, R. A. Crowther, Multiple isoforms of human microtubule-associated protein tau: sequences and localization in neurofibrillary tangles of Alzheimer's disease. *Neuron* **3**, 519–526 (1989).
29. M. Goedert, R. Jakes, Expression of separate isoforms of human tau protein: correlation with the tau pattern in brain and effects on tubulin polymerization. *EMBO J* **9**, 4225–4230 (1990).
30. L. V. C. Miller, A. S. Mukadam, C. S. Durrant, M. J. Vaysburd, T. Katsinelos, B. J. Tuck, S. Sanford, O. Sheppard, C. Knox, S. Cheng, L. C. James, M. P. Coleman, W. A. McEwan, Tau assemblies do not behave like independently acting prion-like particles in mouse neural tissue. *Acta Neuropathol Commun* **9**, 41 (2021).
31. M. Goedert, M. G. Spillantini, N. J. Cairns, R. A. Crowther, Tau proteins of alzheimer paired helical filaments: Abnormal phosphorylation of all six brain isoforms. *Neuron* **8**, 159–168 (1992).
32. T. S. Batth, M. X. Tollenaere, P. Rüther, A. Gonzalez-Franquesa, B. S. Prabhakar, S. Bekker-Jensen, A. S. Deshmukh, J. V Olsen, Protein Aggregation Capture on Microparticles Enables Multipurpose Proteomics Sample Preparation. *Mol Cell Proteomics* **18**, 1027–1035 (2019).
33. C. P. Baker, R. Bruderer, J. Abbott, J. S. C. Arthur, A. J. Brenes, Optimizing Spectronaut Search Parameters to Improve Data Quality with Minimal Proteome Coverage Reductions in DIA Analyses of Heterogeneous Samples. *J Proteome Res* **23**, 1926–1936 (2024).
34. S. Cheng, J. Tereshchenko, V. Zimmer, G. Vachey, C. Pythoud, M. Rey, J. Liefhebber, A. Raina, F. Streit, A. Mazur, M. Bähr, P. Konstantinova, N. Déglon, S. Kügler, Therapeutic efficacy of regulable GDNF

expression for Huntington's and Parkinson's disease by a high-induction, background-free "GeneSwitch" vector. *Exp Neurol* **309**, 79–90 (2018).
35. B. J. Tuck, L. V. C. Miller, T. Katsinelos, A. E. Smith, E. L. Wilson, S. Keeling, S. Cheng, M. J. Vaysburd, C. Knox, L. Tredgett, E. Metzakopian, L. C. James, W. A. McEwan, Cholesterol determines the cytosolic entry and seeded aggregation of tau. *Cell Rep* **39** (2022).
36. G. M. J. Beaudoin, S.-H. Lee, D. Singh, Y. Yuan, Y.-G. Ng, L. F. Reichardt, J. Arikkath, Culturing pyramidal neurons from the early postnatal mouse hippocampus and cortex. *Nat Protoc* **7**, 1741–1754 (2012).

Acknowledgements

We thank Michel Goedert for provision of P301S tau transgenic mice and Reiner Schulte at the CIMR Flow Core Facility for assistance with flow cytometry. We thank the staff at MRC Ares animal facility for animal husbandry and assistance with experimental procedures.

Funding

This study was supported by a Sir Henry Dale Fellowship to W.A.M. jointly funded by the Wellcome Trust and the Royal Society (grant 206248/Z/17/Z) and by the Lister Institute for Preventative Medicine. Further support was provided by the UK Dementia Research Institute (award number UK DRI-2010) through UK DRI Ltd, principally funded by the UK Medical Research Council. J.A.B. was funded by a University of Cambridge MRC Doctoral Training Grant. This work has also received funding from the Innovative Medicines Initiative 2 Joint Undertaking under grant agreement 116060 (IMPRiND). This Joint Undertaking receives support from the European Union's Horizon 2020 research and innovation program and EFPIA. This work is supported by the Swiss State Secretariat for Education, Research and Innovation (SERI) under contract 17.00038. L.C.J., M.V. and L.C.V.M. were supported by a Welcome Trust Investigator Award to L.C.J. (223054/Z/21/Z) and the MRC (UK; U105181010).

This study was supported (to L.B. and I.L.) by the LabEx (Laboratory of Excellence) DISTALZ (Development of Innovative Strategies for a Transdisciplinary approach to Alzheimer's disease ANR-11-LABX-01), and by the ANR (project ToNIC, ANR-18-CE44-0016).

Author contributions

Conceptualisation: J.A.B., L.C.J. & W.A.M.
Methodology: J.A.B., S.C., S.K, D.B., T.K., I.L., E.D., C.D., L.V.C.M. & L.B.
Investigation: J.A.B., S.C., S.K, D.B., T.K., E.D., C.D., A.E.S. & M.J.V.
Funding acquisition: W.A.M.
Supervision: D.K., L.C.J., W.A.M.
Writing – original draft: J.A.B. & W.A.M.
Writing – review and editing: All authors

Competing Interests

None

Data and Materials Availability

All data are available in the manuscript or the supplementary material. Raw data available on written request to W.A.M.

Mass spectrometry raw files and data analysis files produced in Spectronaut have been uploaded to PRIDE (https://doi.org/10.1093/nar/gkab1038) under the accession number PXD052957.

Supplementary Materials

Materials and Methods
Tables S1 to S3
Figs. S1 to S6
Movies S1 to S2

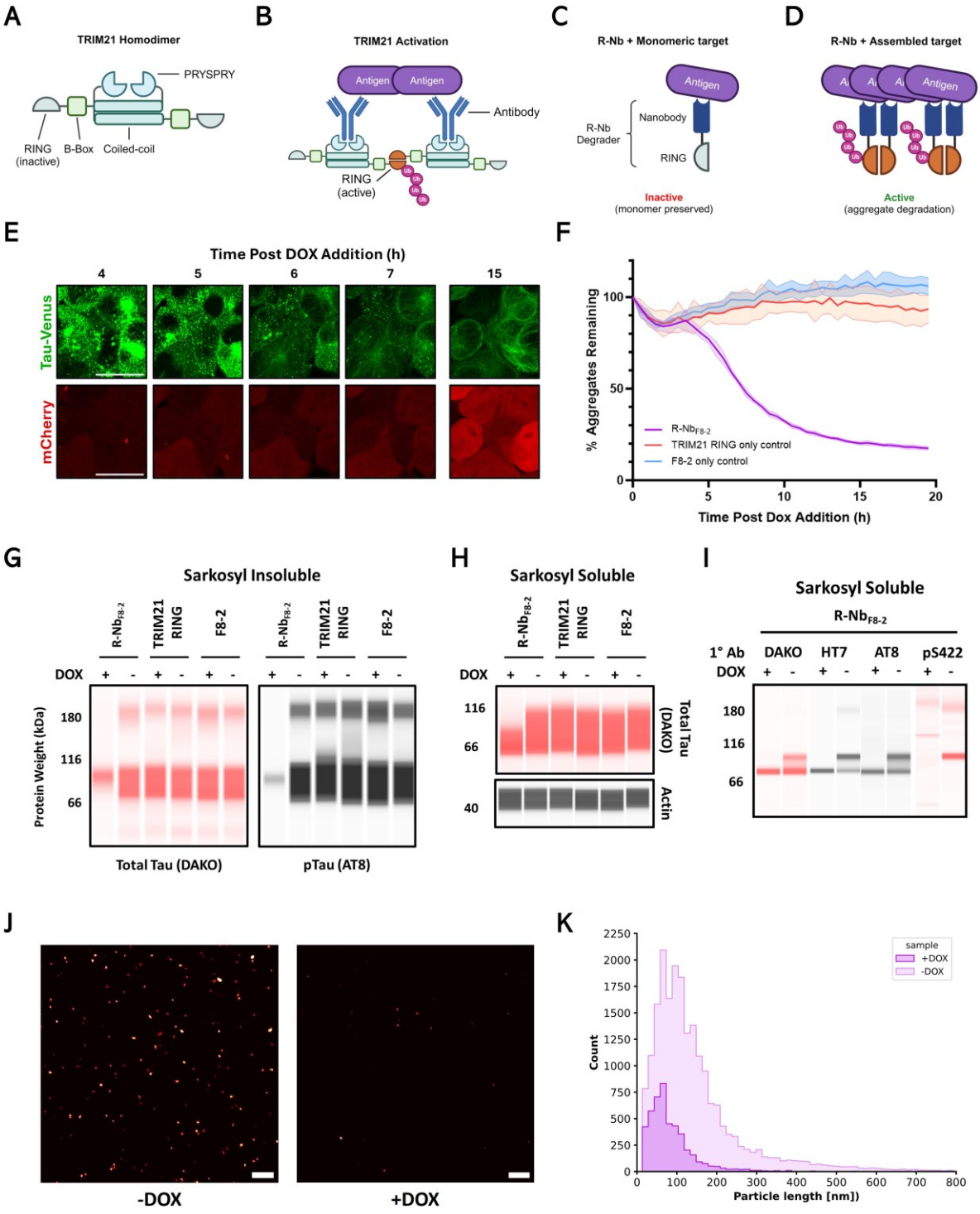
A
TRIM21 Homodimer
PRYSPRY
RING (inactive)
B-Box
Coiled-coil
B
TRIM21 Activation
Antigen
Antigen
Antibody
RING (active)
C
R-Nb + Monomeric target
Antigen
R-Nb Degrader
Nanobody
RING
Inactive
(monomer preserved)
D
R-Nb + Assembled target
Antigen
Active
(aggregate degradation)
E
Time Post DOX Addition (h)
4
5
6
7
15
Tau-Venus
mCherry
F
% Aggregates Remaining
100
50
0
R-Nb$_{F8-2}$
TRIM21 RING only control
F8-2 only control
0
5
10
15
20
Time Post Dox Addition (h)
G
Sarkosyl Insoluble
R-Nb$_{F8-2}$
TRIM21 RING
F8-2
DOX
Protein Weight (kDa)
180
116
66
Total Tau (DAKO)
pTau (AT8)
H
Sarkosyl Soluble
116
66
40
Total Tau (DAKO)
Actin
I
Sarkosyl Soluble
R-Nb$_{F8-2}$
1° Ab
DAKO
HT7
AT8
pS422
DOX
180
116
66
J
-DOX
+DOX
K
sample
+DOX
-DOX
Count
2250
2000
1750
1500
1250
1000
750
500
250
0
0
100
200
300
400
500
600
700
800
Particle length [nm])

Fig. 1. R-Nb$_{F8-2}$ rapidly degrades aggregated tau species.

(**A**) Cytosolic TRIM21 exists as an inactive homodimer, with each monomer consisting of a RING E3 ligase domain, B-Box, Coiled-coil, and an antibody Fc binding PRYSPRY domain. (**B**) The clustering of TRIM21 upon antibody-coated polyvalent substrates allows for RING E3 ligase domain cross-activation and subsequent polyubiquitination. (**C, D**) TRIM21 RING-Nanobody (R-Nb) degraders were engineered to similarly require RING domain cross-activation to induce target degradation and therefore become active upon binding to (D) homotypic assemblies of antigens but not (C) monomeric antigens. (**E**) Live cell fluorescent microscopy of TVA cells which express aggregated P301S tau-venus and DOX-inducible degrader, R-Nb$_{F8-2}$, with an mCherry reporter. Scale bar, 20µm. (**F**) Quantification of tau-venus aggregates from live cell imaging of TVA cells expressing DOX inducible R-Nb$_{F8-2}$, TRIM21 RING, or F8-2. Images were captured and analysed every 30 minutes for 20 hours following DOX addition. (**G**) Capillary based immunoblots of sarkosyl insoluble fractions from TVA cell lines as above treated with or without DOX for 15 hours. Samples were probed for total tau (DAKO) and phospho-tau (pTau) (AT8). (**H**) Sarkosyl soluble fractions from the same experiment were probed for total tau (DAKO) and actin as a loading control. (**I**) Sarkosyl soluble samples were further analysed by diluting 1:4 in PBS and probing with total tau (DAKO and HT7) and pTau (AT8 and pS422) antibodies. (**J**) Representative super-resolution microscopy images of tau-venus aggregates in lysates from TVA cells expressing DOX inducible R-Nb$_{F8-2}$ treated with or without DOX for 15 hours, using anti-tau antibody HT7 for both capture and detection. Scale bar, 1µm (**K**) Histogram showing the size and count of tau-venus aggregates detected from super-resolution microscopy images. Shaded areas represent mean ± SD. (F) n = 8 biological replicates per condition. (K) n = 6 technical replicates per condition.

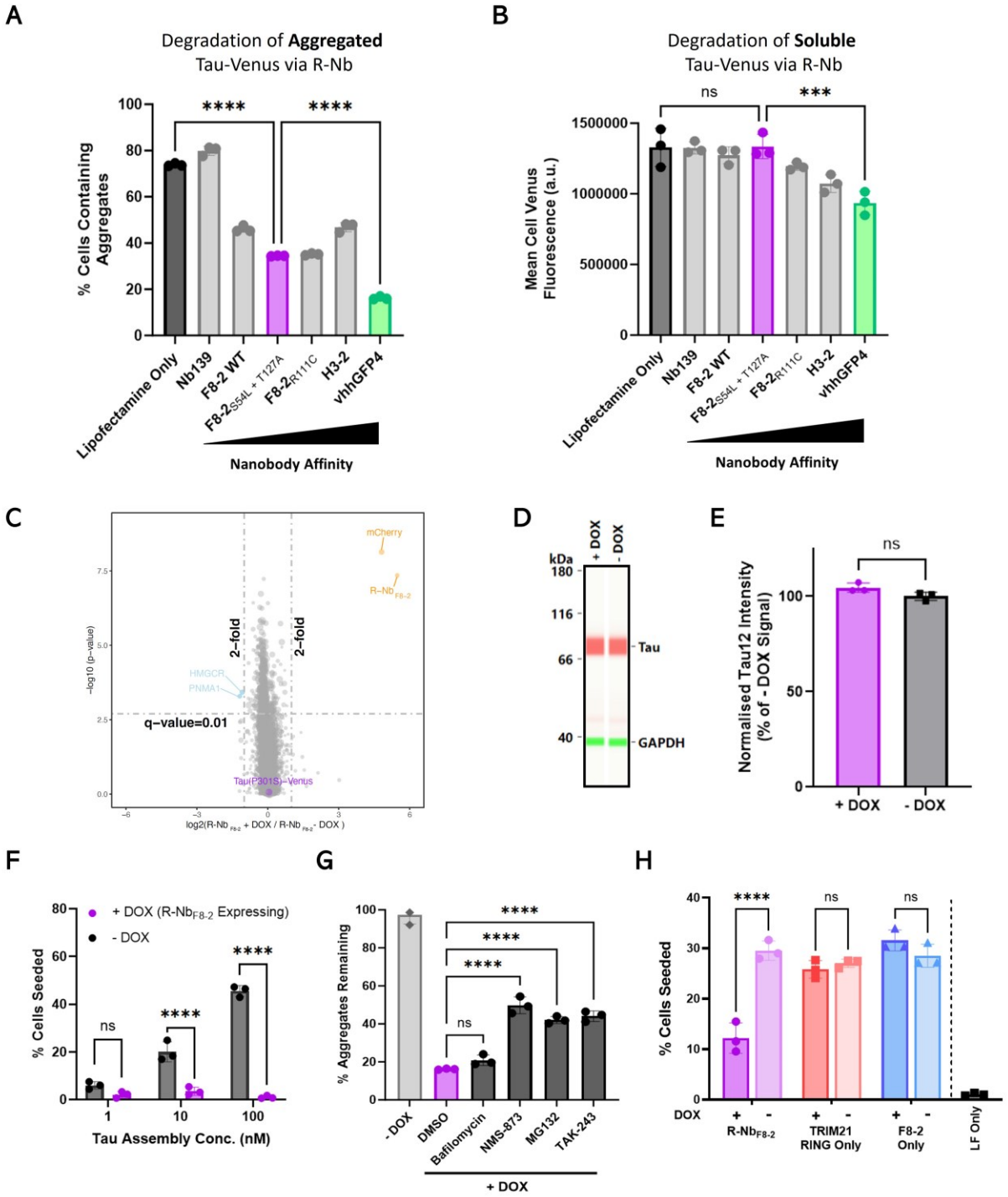
A
Degradation of Aggregated Tau-Venus via R-Nb
% Cells Containing Aggregates
Lipofectamine Only
Nb139
F8-2 WT
F8-2S54L + T127A
F8-2R111C
H3-2
vhhGFP4
Nanobody Affinity
B
Degradation of Soluble Tau-Venus via R-Nb
Mean Cell Venus Fluorescence (a.u.)
ns
***
C
mCherry
R-NbF8-2
2-fold
2-fold
HMGCR
PNMA1
q-value=0.01
Tau(P301S)-Venus
D
kDa
+ DOX
- DOX
Tau
GAPDH
E
Normalised Tau12 Intensity (% of - DOX Signal)
F
+ DOX (R-NbF8-2 Expressing)
- DOX
% Cells Seeded
Tau Assembly Conc. (nM)
G
% Aggregates Remaining
- DOX
DMSO
Bafilomycin
NMS-873
MG132
TAK-243
+ DOX
H
% Cells Seeded
DOX
R-NbF8-2
TRIM21 RING Only
F8-2 Only
LF Only

Fig. 2. Selective degradation of aggregated tau by R-Nb is dependent on nanobody affinity and protects cells against seeded tau aggregation.

(**A**) TVA cells were transfected with R-Nb plasmids employing nanobodies of varying in vitro affinities for tau-venus. F8-2 WT (1332 nM), F8-$2_{S54L+T127A}$ (683 nM), F8-2_{R111C} (211 nM), H3-2 (32 nM), vhhGFP4 (1 nM) or Nb139 (p53 targeting, negative control). 24 hours post-transfection the percentage of cells containing aggregated tau-venus was quantified via fluorescence microscopy. (**B**) TVS cells were transfected with the same R-Nb plasmids, with venus fluorescence quantified by flow-cytometry 24 hours post-transfection. (**C**) DOX inducible R-Nb_{F8-2} TVA cells were lysed 15 hours post-DOX addition, and their proteome compared to untreated (-DOX) cells via mass spectrometry. Significantly altered proteins (q-value <0.01, fold change >2 or <-2) are labeled, alongside TauP301S-Venus. (**D**) Immunoblot of lysates from DOX inducible R-Nb_{F8-2} TVS cells, 24 hours after +/- DOX treatment. Samples probed for tau (Tau12 antibody) and GAPDH. (**E**) Levels of tau, normalised to GAPDH, in TVS cells + DOX relative to – DOX levels. (**F**) TVS cells pretreated +/- DOX for 24 hours were challenged with heparin assembled P301S tau assemblies. Percentage of cells containing tau-venus aggregates quantified 72 hours later via fluorescent microscopy. (**G**) Percentage of tau-venus aggregates remaining in TVA cells expressing DOX inducible R-Nb_{F8-2}, treated with E1/Proteasome/VCP/autophagy inhibitors (solubilised in DMSO) and DOX for 10 hours, compared to TVA without DOX, quantified by fluorescence microscopy. TAK-243, 100 nM; MG132, 125 nM; NMS-873, 5 μM; Bafilomycin A1, 400 nM. (**H**) Lysates from TVA cells expressing DOX inducible R-Nb_{F8-2}, or RING/F8-2 only controls, treated +/- DOX for 15 hours, were introduced to TVS cells via Lipofectamine (LF). Seeded aggregation of tau-venus was quantified 72 hours later via fluorescent microscopy. Error bars indicate mean ± SD. (A), (B), (E), (F), (G) and (H) n = 3 biological replicates. (C) n = 3 technical replicates. (A), (B), (G) and (H) one-way analysis of variance (ANOVA) with Tukey's correction for multiple comparisons. (E) unpaired *t* test. (F) two-way ANOVA with Šídák's correction for multiple comparisons. ns, not significant; ***$P < 0.001$; ****$P < 0.0001$.

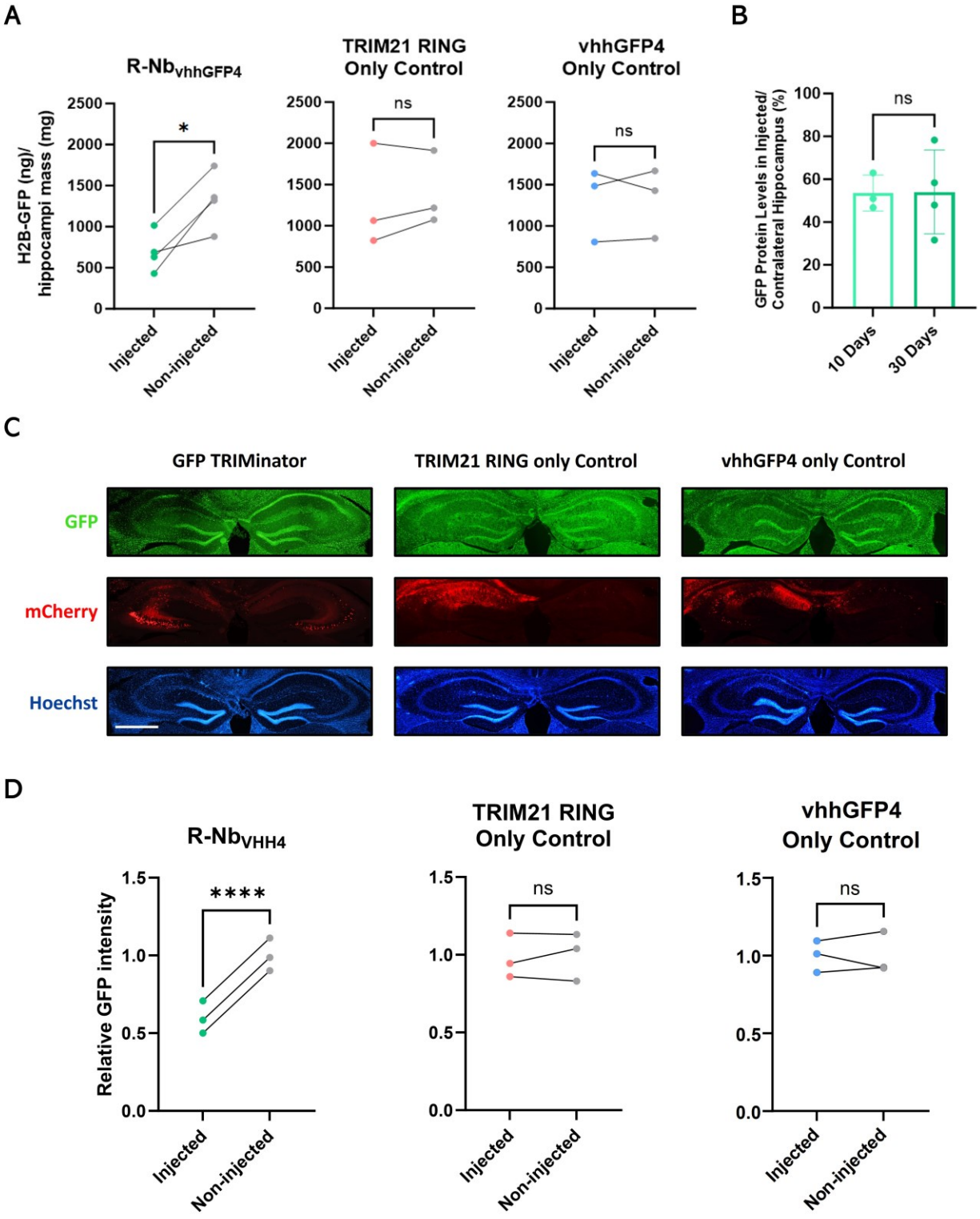
A
R-Nb$_{vhhGFP4}$
TRIM21 RING Only Control
vhhGFP4 Only Control
H2B-GFP (ng)/ hippocampi mass (mg)
2500
2000
1500
1000
500
0
*
ns
ns
Injected
Non-injected
B
GFP Protein Levels in Injected/ Contralateral Hippocampus (%)
100
80
60
40
20
0
ns
10 Days
30 Days
C
GFP TRIMinator
TRIM21 RING only Control
vhhGFP4 only Control
GFP
mCherry
Hoechst
D
R-Nb$_{VHH4}$
TRIM21 RING Only Control
vhhGFP4 Only Control
Relative GFP intensity
1.5
1.0
0.5
0.0
****
ns
ns
Injected
Non-injected

5

Fig. 3. In vivo degradation of H2B-GFP in the mouse brain using R-Nb$_{vhhGFP4}$.

(**A**) H2B-GFP protein levels in hippocampi of transgenic H2B-GFP mice unilaterally injected at two months of age with $2x10^9$ genome copies (GC) AAV1/2 (encoding R-Nb$_{vhhGFP4}$, TRIM21 RING, or vhhGFP4) compared to non-injected contralateral hippocampi, quantified via GFP ELISA and normalised to hippocampus mass. (**B**) Comparison of H2B-GFP protein levels in hippocampi injected with AAV1/2 R-Nb$_{vhhGFP4}$ for 10 or 30 days, quantified via ELISA and presented as percentage H2B-GFP protein compared to non-injected contralateral hippocampi. (**C**) Representative fluorescent microscopy images of hippocampi injected with AAV1/2 encoding R-Nb$_{vhhGFP4}$, TRIM21 RING, or vhhGFP4 30 days post-injection. Scale bar, 1mm. (**D**) GFP intensity in AAV1/2 injected vs non-injected hippocampi was quantified from fluorescent microscopy images and normalised against the average signal in non-injected hippocampi. (A) and (B) each point represents the average of two technical replicates from one mouse. n = 3 or 4 mice. (D) each point represents the average of 4 brain slices from one mouse. n = 3 mice. (A) and (D) paired *t* test, (B) un-paired *t* test. ns, not significant; $*P < 0.05$; $****P < 0.0001$.

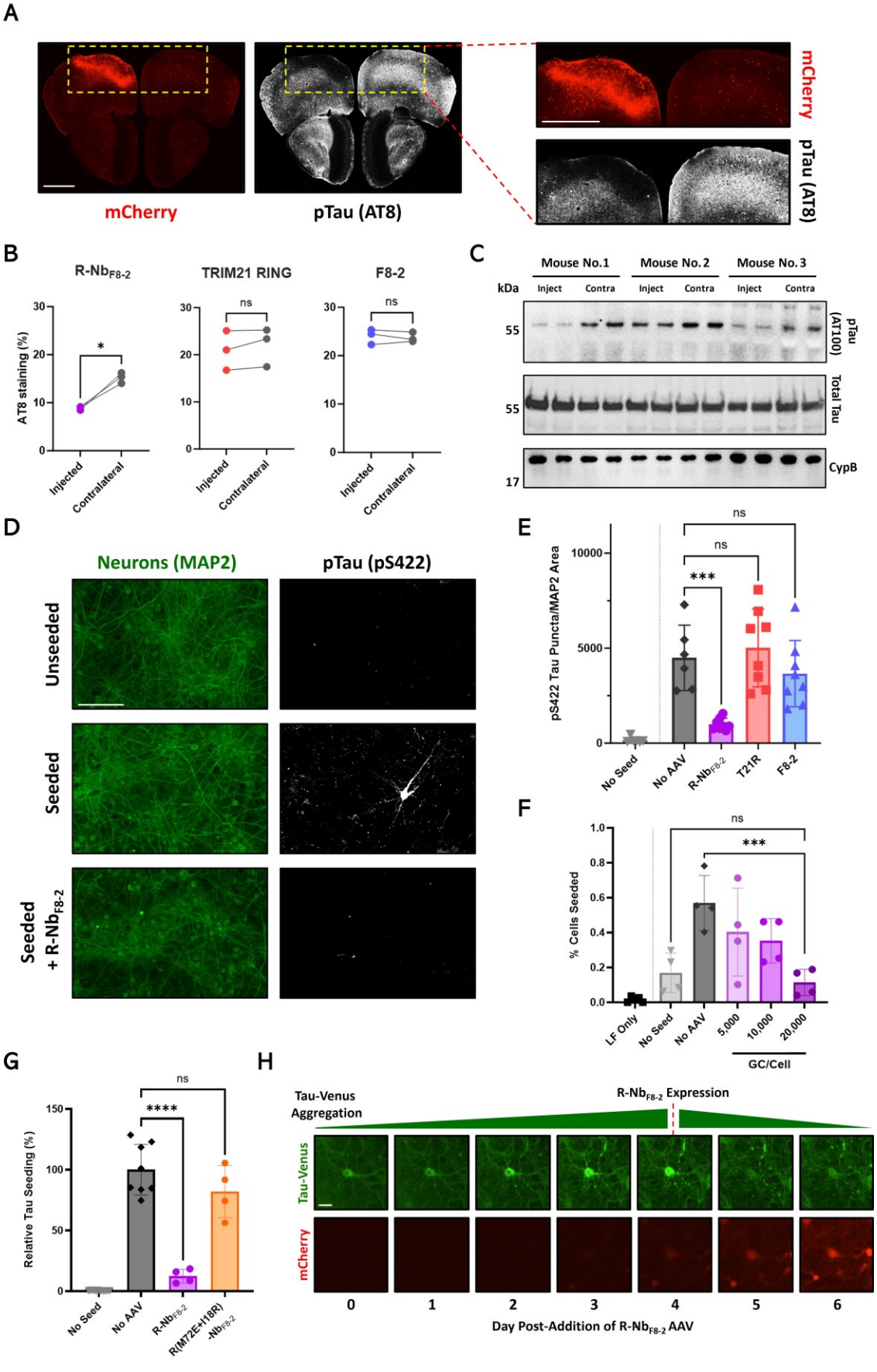
A
mCherry
pTau (AT8)
mCherry
pTau (AT8)
B
R-Nb$_{F8-2}$
TRIM21 RING
F8-2
AT8 staining (%)
ns
*
Injected
Contralateral
C
Mouse No.1
Mouse No. 2
Mouse No. 3
kDa
Inject
Contra
55
pTau (AT100)
Total Tau
17
CypB
D
Neurons (MAP2)
pTau (pS422)
Unseeded
Seeded
Seeded + R-Nb$_{F8-2}$
E
pS422 Tau Puncta/MAP2 Area
ns
***
No Seed
No AAV
R-Nb$_{F8-2}$
T21R
F8-2
F
% Cells Seeded
LF Only
5,000
10,000
20,000
GC/Cell
G
Relative Tau Seeding (%)
****
R(M72E+I18R)-Nb$_{F8-2}$
H
Tau-Venus Aggregation
R-Nb$_{F8-2}$ Expression
Tau-Venus
mCherry
Day Post-Addition of R-Nb$_{F8-2}$ AAV

Fig. 4. Reduction of tau pathology in the aged mouse brain and primary neurons via R-Nb$_{F8-2}$.

(**A**) Representative IF images 30 days post-stereotaxic injection of AAV1/2-CAG-R-Nb$_{F8-2}$-T2A-mCherry into the left frontal cortex (two 2x10^9 GC doses) of 5.5-month-old Tg2541 mice. pTau detected using AT8. Scale bars, 1mm. (**B**) Quantification of AT8 coverage in AAV1/2 injected vs contralateral frontal cortex hemispheres, 10 days post-injection. (**C**) Western blot of injected and contralateral cortical hemisphere lysates 10 days after injection with R-Nb$_{F8-2}$ AAV1/2. Samples ran in duplicate and probed for pTau, total tau, and loading control with AT100, BR134 and CypB antibodies respectively. (**D**) Representative IF images of primary Tg2541 mouse neuron cultures, "seeded" via addition of 50 nM heparin-assembled P301S tau assemblies 7 days after pre-treatment with AAV1/2-hSyn-R-Nb$_{F8-2}$-T2A-mCherry (20,000 GC/cell). pTau aggregates detected 7 days post-seeding via anti-pTau pS422 staining, with neurons identified via MAP2 staining. Scale bar, 100µm. (**E**) Quantification of pS422 tau puncta normalised against MAP2 coverage from IF images. Seeded neurons were pre-treated with AAV1/2 encoding R-Nb$_{F8-2}$, TRIM21 RING (T21R) or F8-2 only. (**F**) Lysates from tau seeded neurons pre-treated with R-Nb$_{F8-2}$ AAV1/2 (various GC doses) were introduced to TVS cells via Lipofectamine (LF). Tau-venus aggregation was quantified 72 hours later via fluorescent microscopy. (**G**) Relative levels of pS422 tau puncta (normalised against MAP2 coverage) in tau seeded neurons pre-treated with catalytically dead or active R-Nb$_{F8-2}$ AAV1/2 (20,000 GC/cell), compared to untransduced neurons. (**H**) Primary C57BL/6 mouse neuron cultures were transduced with AAV1/2-hSyn-0N4R P301S tau-venus (20,000 GC/cell), seeded 7 days later with heparin assembled P301S tau assemblies, then transduced 3 days post-seeding with R-Nb$_{F8-2}$ AAV1/2 (20,000 GC/cell), after which images were captured via live cell imaging. Scale bar, 20µm. Error bars represent mean ± SD. (B) n = 3 mice, 4 technical repeats per point. (E) and (G) n = 4 - 8 biological repeats, 2 technical repeats per point. (F) n = 4 biological repeats. (B) Paired *t* test. (E), (F) and (G) ANOVA with Tukey's correction for multiple comparisons. ns, not significant; *$P < 0.05$; ***$P < 0.001$; ****$P < 0.0001$.

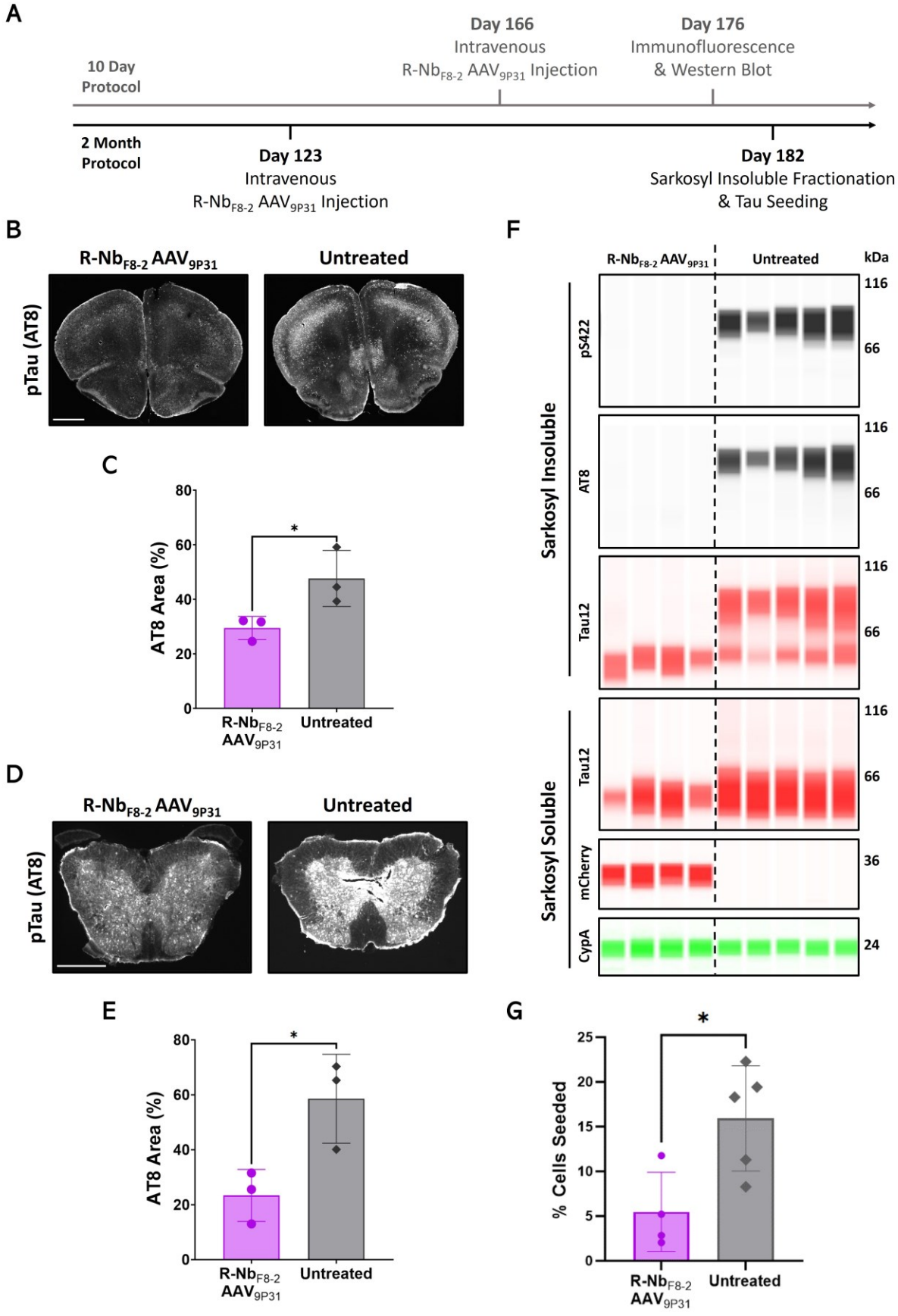
A
10 Day Protocol
Day 166
Intravenous
R-Nb$_{F8-2}$ AAV$_{9P31}$ Injection
Day 176
Immunofluorescence
& Western Blot
2 Month Protocol
Day 123
Intravenous
R-Nb$_{F8-2}$ AAV$_{9P31}$ Injection
Day 182
Sarkosyl Insoluble Fractionation
& Tau Seeding
B
R-Nb$_{F8-2}$ AAV$_{9P31}$
Untreated
pTau (AT8)
C
AT8 Area (%)
R-Nb$_{F8-2}$ AAV$_{9P31}$
Untreated
D
R-Nb$_{F8-2}$ AAV$_{9P31}$
Untreated
pTau (AT8)
E
AT8 Area (%)
R-Nb$_{F8-2}$ AAV$_{9P31}$
Untreated
F
R-Nb$_{F8-2}$ AAV$_{9P31}$
Untreated
kDa
Sarkosyl Insoluble
pS422
AT8
Tau12
Sarkosyl Soluble
Tau12
mCherry
CypA
116
66
36
24
G
% Cells Seeded
R-Nb$_{F8-2}$ AAV$_{9P31}$
Untreated

Fig. 5. Global CNS expression of R-Nb$_{F8-2}$ reduces tau pathology in mice.

(**A**) Timeline of short (10 day) and long (2 month) experimental protocol using R-Nb$_{F8-2}$ AAV$_{9P31}$ in Tg2541 mice. In both scenarios mice were treated with a single dose of 1x10^{11} GC of R-Nb$_{F8-2}$ AAV$_{9P31}$ via tail vein injection. (**B**) Representative IF images of frontal cortices stained with AT8 from aged mice treated with or without R-Nb$_{F8-2}$ AAV$_{9P31}$ for 10 days. Scale bar, 1mm (**C**) Quantification of AT8 coverage from IF images in (B). (**D**) Representative IF images of spinal cords from the same mice, stained for AT8. Scale bar, 0.5mm (**E**) Quantification of AT8 staining in spinal cord sections (D). (**F**) Sarkosyl soluble and insoluble fractions were prepared from whole brains of aged mice treated with or without 1x10^{11} GC R-Nb$_{F8-2}$ AAV$_{9P31}$ for two months. Insoluble fractions were blotted for pTau (pS422 and AT8) and total tau (Tau12), with soluble fractions blotted for Tau12 and mCherry, with CypA as a loading control. Each lane represents an individual mouse. (**G**) Levels of seeded tau aggregation in TVA cells treated with brain homogenates from aged mice treated with or without R-Nb$_{F8-2}$ AAV$_{9P31}$ for two months. Error bars represent mean ± SD. (C) and (E) each point represents the average of 4 brain slices from one mouse. n = 3 mice. (G) Each point represents the average percentage of TVS cells seeded (6 technical replicates) by homogenate from one mouse. n = 4 or 5 mice. Unpaired *t* test, $*P < 0.05$.

Science
AAAS

Supplementary Materials for

Aggregate-selective removal of pathological tau via clustering-activated degraders

Jonathan Benn*[1†], Shi Cheng*[1†], Sophie Keeling[1], Annabel E Smith[1], Marina J Vaysburd[2], Dorothea Böken[1], Lauren VC Miller[2], Taxiarchis Katsinelos[1,2], Catarina Franco[2], Elian Dupré[3,4], Clément Danis[3,4,5], Isabelle Landrieu[3,4], Luc Buée[5], David Klenerman[1], Leo C James*[2,] William A McEwan*[1]

Corresponding authors: J.B: jb2310@cam.ac.uk. S.C: chengshi1013@163.com. W.M: wm305@cam.ac.uk. L.J: lcj@mrc-lmb.cam.ac.uk.

The PDF file includes:

Materials and Methods
Tables S1 to S3
Figs. S1 to S6

Other Supplementary Materials for this manuscript include the following:

Movies S1 to S2

Materials and Methods

Cloning

TRIM21 RING-Nanobody-T2A-mCherry (R-Nb) constructs were created using residues 1-85 of TRIM21 (encoding the RING E3 ligase domain) followed by a GGGGS linker connecting to the nanobody sequence. A C-terminal self-cleaving mCherry tag was added via inclusion of a T2A peptide (GSGEGRGSLLTCGDVEENPGP) prior to the mCherry sequence. R-Nb constructs were subcloned into pcDNA3.1+ (ThermoFisher, V79020) and pcDNA4.0/TO (ThermoFisher, V102020) for transient transfection and generation of doxycycline inducible cell lines respectively. R-Nb constructs were also subcloned into pAAV-CAG-GFP (Addgene plasmid #37825) and pAAV-hSYN-EGFP (Addgene plasmid #50465) vectors, replacing the GFP/EGFP transgene, for production of AAV particles carrying the R-Nb transgene.

Nanobody sequences used in R-Nb constructs (Table 1) were identified from the literature and synthesised as DNA fragments (GeneArt Strings, ThermoFisher) or generously provided by Elian Dupré and Luc Buée. Site directed mutagenesis (SDM) was used to make F8-2 variants.

Nanobody (Nb)	Target	Affinity (nM)	Reference
vhhGFP4	GFP	1	Kubala et al., 2010
MDQVQLVESGGALVQPGGSLRLSCAASGFPVNRYSMRWYRQAPGKEREWVAGMSSAGDRSSYEDSVKGRFTISRDD ARNTVYLQMNSLKPEDTAVYYCNVNVGFEYWGQGTQVTVSS			
F8.2	Tau	1332	Dupré et al., 2019
MAEVQLQASGGGFVQPGGSLRLSCAASGGTSYWDGMGWFRQAPGKEREFVSAISGRGNIGTYYADSVKGRFTISRD NSKNTVYLQMNSLRAEDTATYYCAAFRHEVHGSMRHEWEVIKYWGQGTQVTVSS			
F8.2 S54L T127A	Tau	683	Dupré et al., 2019, Fig. S2D
MAEVQLQASGGGFVQPGGSLRLSCAASGGTSYWDGMGWFRQAPGKEREFVSAI**L**GRGNIGTYYADSVKGRFTISRD NSKNTVYLQMNSLRAEDTATYYCAAFRHEVHGSMRHEWEVIKYWGQGTQV**A**VSS			
F8.2 R111C	Tau	211	Dupré et al., 2019
MAEVQLQASGGGFVQPGGSLRLSCAASGGTSYWDGMGWFRQAPGKEREFVSAISGRGNIGTYYADSVKGRFTISRD NSKNTVYLQMNSLRAEDTATYYCAAFRHEVHGSM**C**HEWEVIKYWGQGTQVTVSS			
H3-2	Tau	32	Fig. S2 A-C
MAEVQLQASGGGFVQPGGSLRLSCAASGYTSGDEIMGWFRQAPGKEREFVSAISWQSGTSTYYADSVKGRFTISRD NSKNTVYLQMNSLRAEDTATYYCAPMTLAETYYEWLISGYWGQGTQVTVSS			
Nb139	p53	N/A (for Tau-Venus)	Bethuyne et al., 2014
AQVQLQESGGGLVQAGGSLRLSCAASERTFSTYAMGWFRQAPGREREFLAQINWSGTTTYYAESVKDRTTISRDNA KNTVYLEMNNLNADDTGIYFCAAHPQRGWGSTLGWTYWGQGTQVTVSS			

Table S1. Nanobodies (Nb) used in R-Nb constructs.

Nanobody name, target, affinity and reference are given along with protein primary sequence. Bold residues indicate mutations in F8-2 variants.

Cell line creation and culture

HEK293 T-REx cells (ThermoFisher, R71007) were cultured in complete DMEM supplemented with 10% vol/vol foetal bovine serum (FBS), 100 U/ml penicillin and 100 µg/ml streptomycin at 37°C with 5% CO2 in a humid atmosphere. TVS cells expressing soluble human 0N4R P301S tau with a C-terminal venus fluorophore (*8*) were transfected with sarkosyl insoluble tau assemblies isolated from 6 month old Tg2541 P301S tau transgenic mice and clonally selected to isolate a line in which tau-venus was constitutively aggregated (TVA cells).

TVS and TVA cells expressing DOX inducible R-Nb constructs were created by stable transfection with R-Nb pcDNA4/TO plasmids using Lipofectamine 3000 (ThermoFisher, L3000015), followed by selection in media containing 50µg/ml Zeocin (AlfaAesar, J67140). Construct expression was induced via the addition of 1µg/ml DOX (MP Biomedicals), 195044) in the media. Small molecule inhibitors of the UPS/VCP/Autophagy (solubilised in DMSO) were added at the following concentrations in the media alongside 1µg/ml DOX: TAK-243 (100nM); HOIPIN-8 (25µM); MG132 (125nM); NMS-873 (5µM); Bafilomycin A1 (400nM).

Recombinant tau protein production

The expression and purification of recombinant human 6xHis-0N4R tau bearing the P301S mutation from E. coli BL-21 (DE3, Agilent Technologies) was performed as described previously (*28*, *29*) with small modifications. Bacterial pellets were collected through centrifugation (3300 g, 4 °C, 10 min) and then resuspended in 10 ml/L of culture with buffer A (25 mM HEPES, pH 7.4, 300 mM NaCl, 20 mM Imidazole, 1 mM benzamidine, 1 mM PMSF, 14 mM β-mercaptoethanol, 1% NP-40, 1 x complete EDTA-free protease inhibitors). The resuspended bacteria were lysed on ice using a probe sonicator and boiled for 10 min at 95 °C which denatures the majority of proteins, but not tau. Denatured proteins were pelleted by ultracentrifugation at 100,000 g, 4 °C for 50 min. The clarified supernatant containing 6xHistagged monomeric tau P301S was then passed through a HisTrap FF column according to manufacturer instructions (GE Healthcare). Eluted fractions were assessed through SDS-PAGE and total protein staining with Coomassie InstantBlue. Fractions of interest were concentrated using 10 kDa cut-off Amicon Ultra-15 concentrators (Merck Millipore) before loading on a HiLoad 16/600 Superdex 200 (Cytiva) size exclusion chromatography column. To remove the 6xHis tag, tau was subjected to TEV protease following manufacturer's instructions (Sigma-Aldrich, T4455). After incubation, the pooled fractions were loaded onto a second HisTrap HP column to remove protease and the successfully cleaved tau collected. Cleaved tau was concentrated using a 10 kDa cut-off Amicon Ultra-15 concentrator (Merck Millipore) before loading onto a HiLoad 16/600 Superdex 200 (Cytiva) size exclusion chromatography column. All purification was performed on an ÄKTA Pure system (Cytiva). Purified tau was concentrated to at least 3 mg/mL using a 10 kDa cut off AmiconUltra-15 concentrator (Merck Millipore) and snapfrozen in liquid nitrogen for storage at -80 °C in PBS containing 1 mM DTT. Levels of endotoxin were measured using a limulus amebocyte lysate kit and found to be below 0.01 EU/ml at tau concentrations used in experiments.

In vitro aggregation of recombinant tau protein

Tau monomer was aggregated as described previously (*28*). Briefly, 60 μM tau monomer was incubated with 20 μM heparin, 2 mM DTT and 1X protease inhibitors in PBS for 24–72 h at 37°C shaking at 250 RPM. Thioflavin T (ThT, Thermo Fisher, T3516) was used to quantify Tau aggregation. Tau assemblies were then diluted in PBS to 20 μM monomer equivalent, snap-frozen in liquid nitrogen and stored at -80 °C.

Quantification of tau-venus aggregation in cell lines via fluorescent microscopy

20,000 TVA cells per well of a 96-well plate were reverse transfected with pcDNA3.1+ plasmids encoding R-Nb constructs. 24 hours later, live cells were washed 2x with PBS and incubated with 2μg/ml Hoechst (Invitrogen, H3570) in PBS for 30 minutes at 37°C. Images were then acquired on an Eclipse Ti2 Microscope (Nikon) using a 10x objective with the percentage of cells containing tau-venus aggregates, and mean cell mCherry fluorescence, being quantified using NIS-elements software (Nikon). Quantitative live cell imaging of TVA cells expressing DOX inducible constructs was performed similarly, with cells being plated the day before DOX addition and then imaged every 30 minutes post-DOX addition for 20 hours. Videos and representative images were acquired from cells cultured on glass coverslips and imaged on a confocal microscope (STELLARIS8, Leica), with images being acquired every 20 minutes from 4 to 15 hours post DOX addition.

Seeded tau aggregation in TVS cells induced by heparin assembled tau assemblies was performed largely as described previously (*8*). 15,000 TVS cells were plated per well of a 96-well plate in 50μL OptiMEM (ThermoFisher, 31985070) and treated with varying concentrations of tau assemblies diluted in a further 50μL OptiMEM containing 0.5μL Lipofectamine 2000 (ThermoFisher, 11668019). After 1 hour, 100μL complete DMEM was added to each well to stop the transfection process. 72 hours later, live cells were washed 2x with PBS and incubated with 2μg/ml Hoechst (Invitrogen, H3570) in PBS for 30 minutes at 37°C. Images were then acquired on an Eclipse Ti2 Microscope using a 10x objective with the percentage of cells containing tau-venus aggregates being quantified using NIS-elements software.

A similar protocol was used to quantify seeded tau aggregation induced by various homogenate samples. HEK293 and neuronal cultures were lysed via the addition of ice-cold PBS containing 1x Halt™ protease and phosphatase inhibitor cocktail (ThermoFisher, 78440) and 5 cycles of freeze-thaw between -80°C and 37°C, after which membranes were pelleted and supernatants collected. The preparation of mouse brain homogenates is described later (*Preparation of homogenates and sarkosyl soluble and insoluble fractions from HEK293T cells and mouse brains*). The total protein concentration in all homogenates was quantified via BCA and adjusted with PBS to 20ng/μL for samples from HEK293 and neuronal cultures, and to 100ng/μL for mouse brain homogenates. Samples were then transfected into TVS cells following the same protocol as transfection of heparin assembled tau assemblies.

Flow Cytometry

100,000 TVS cells were plated per well of a 24-well plate and reverse transfected with pcDNA3.1+ plasmids encoding R-Nb constructs. 24 hours later, cells were collected into a round bottom 96-well plate, pelleted, and then resuspended in 150µL PBS. This plate was loaded into a CytoFLEX (Beckman Coulter) flow cytometer where 10,000 events per condition were recorded. Cells were gated to be live singlets and have equal mean mCherry expression, with analysis and gating being performed on CytExpert software (Beckman Coulter).

Preparation of homogenates and sarkosyl soluble and insoluble fractions from HEK293T cells and mouse brains

HEK293 homogenates were prepared via addition of M-PER™ Mammalian Cell Lysis Buffer (ThermoFisher, 78501) followed by one freeze-thaw cycle between -80°C and room temperature. Lysates were cleared by centrifugation and supernatants collected for analysis.

Mouse brains were homogenised in ice-cold H-Buffer (10 mM Tris pH 7.4, 1 mM EGTA, 0.8 M NaCl, 10% w/v sucrose, 1x protease and phosphatase inhibitors) in a 6:1 volume (µL):brain mass (mg) ratio using the VelociRuptor V2 Microtube Homogeniser (Scientific Laboratory Supplies). Homogenisation was completed with a KIMBLE® pestle homogeniser (DWK Life Sciences) prior to samples being lysed by sonication and clarified by centrifugation.

Sarkosyl soluble and insoluble fractions were extracted from HEK293 cells (TVA), and mouse brain homogenates as previously described (*30*). TVA cell homogenates were prepared by resuspending cells (from one 10cm dish) in 1ml H-Buffer (plus 1% Sarkosyl), then lysing cells via sonication. Mouse brain homogenates, prepared as described above, had sarkosyl added up to a final concentration of 1%. To isolate sarkosyl soluble and insoluble fractions from these homogenates (TVA or mouse brain), samples were incubated for 1 hour at 37°C and then centrifuged at 100,000x g for 1 hour at 4°C. Sarkosyl soluble fractions were collected and the resulting sarkosyl insoluble pellet was resuspended in 15µL tris-buffered saline (TBS) for TVA samples, and in 0.2ml/gram of original brain tissue for mouse brain derived samples, after which all samples were sonicated before storage at -80°C.

Capillary-based immunoblot

Proteins of interest in homogenates or sarkosyl soluble/insoluble fractions from HEK293 cells or mouse brain samples were detected using the automated Jess capillary-based immunoblot platform (Bio-Techne). Samples were mixed with Jess 5x fluorescent master mix and boiled at 100°C for 5 minutes, with 4µL of sample then being ran on the Jess system as per the manufacturer's instructions. Primary and Secondary antibodies used are described in Table 2. Band intensities were quantified using Simple Western software (Bio-Techne).

Antibody Target	Antibody Species	Antibody Dilution	Supplier & Catalogue No.
Total Tau (Tau12)	Mouse	1:100	Sigma-Aldrich, MAB2241
Total Tau (DAKO)	Rabbit	1:100	Dako, A0024
Total Tau (HT7)	Mouse	1:100	Invitrogen, MN1000
pTau (AT8)	Mouse	1:25	Invitrogen, MN1020
pS422	Rabbit	1:25	Abcam, ab79415
pS396	Rabbit	1:15	Invitrogen, 44-752G
mCherry	Rabbit	1:50	Proteintec, 26765-1-AP
GAPDH	Rabbit	1:100	Bio-Techne, 2275-PC-100
Actin	Mouse	1:50	Bio-Techne, MAB8929
CypA	Goat	1:40	Bio-Techne, AF3589
2A Peptide	Mouse	1:25	Merck, MABS2005
Anti-Mouse IgG (647 Secondary)	Donkey	1:20	Invitrogen, A32787
Anti-Mouse IgG (HRP Secondary)	Donkey	1:20	Invitrogen, A16017
Anti-Rabbit IgG (800 Secondary)	Donkey	1:20	Invitrogen, A32808
Anti-Rabbit IgG (647 Secondary)	Donkey	1:20	Invitrogen, A32795
Anti-Rabbit IgG (HRP Secondary)	Donkey	1:20	Jackson, 711-035-152
Anti-Goat IgG (800 Secondary)	Donkey	1:20	Rockland, 605-745-125

Table S2. List of primary and secondary antibodies used with automated Jess capillary-based immunoassay system.

Western Blot

Proteins of interest in HEK293 cell or mouse brain homogenates were also detected via western blot. 4x NuPAGE LDS sample buffer (ThermoFisher, NP0007) with 2mM β-mercaptoethanol was added to samples before boiling for 5 mins, after which samples were subjected to SDS-PAGE using NuPAGE Bis-Tris 4-12% gels (ThermoFisher, NP0324BOX) and transferred to 0.2µm PVDF membrane using the Bio-Rad Transblot Turbo Transfer System. Membranes were blocked in 5% milk with 0.2x fish gelatine in TBS-T (0.1% Tween-20 in TBS) for 1 hour at room temperature before incubation with primary antibodies (Table 3). Membranes were incubated in primary antibody overnight at 4 ºC and following repeated washes with TBS-T, were incubated with secondary antibodies (Table 3) for 1 hour at room temperature. Membranes then washed with TBS-T and incubated with HRP substrate where appropriate (Millipore, WBKLS0500), before imaging on a ChemiDoc system (BioRad). Band intensities were quantified using ImageJ Software.

Antibody Target	Antibody Species	Antibody Dilution	Supplier & Catalogue No.
pTau (AT100)	Mouse	1:1000	Invitrogen, MN1060
Total Tau (BR134)	Rabbit	1:1000	Goedert et al., 1989
CypB	Mouse	1:5000	Santa Cruz, K2E2
Ubiquitin	Mouse	1:2000	ThermoFisher, MA1-10035
LC3B	Rabbit	1:1000	Merck, L7543
GAPDH	Mouse	1:5000	Abcam, Ab8245
Mouse IgG (HRP Secondary)	Goat	1:8000	Invitrogen, A16011
Rabbit IgG (HRP Secondary)	Goat	1:8000	Invitrogen, A16023
Mouse IgG (Dylight 800 Secondary)	Goat	1:5000	ThermoFisher, SA5-10176
Rabbit IgG (Dylight 800 Secondary	Goat	1:5000	ThermoFisher, SA5-10036

Table S3. List of primary and secondary antibodies used for western blot.

Immuno-gold electron microscopy

Sarkosyl insoluble species from TVA cells were applied on glow-discharged 400 mesh formvar/carbon film-coated copper grids (EM Sciences, CF400-Cu) for 45 secs. Immunogold labelling was performed as described previously (*31*). Briefly, grids with deposited samples were blocked at room temperature for 10 min with PBS + 0.1% fish gelatine (G7041, Merck) and then incubated with anti-tau (BR134) (*28*) or anti-GFP (Ab6556, Abcam) antibodies diluted in blocking buffer (1:50) for 1 hour at room temperature. Grids were subsequently washed with blocking buffer and incubated with 10nm gold-conjugated anti-rabbit IgG secondary antibody (G7402, Merck) for 1 h at room temperature diluted 1:20 in blocking buffer. Grids were finally washed with water, stained with 2% uranyl-acetate for 45 secs and air-dried for at least 30 min before imaging. Images were acquired at 4,400× and 6,500× with a defocus value of -1.4 µm with Gatan Orius SC200B detector using a Tecnai G2 Spirit at 120 kV.

Single molecule pull-down (SiMPull) super-resolution microscopy

Single molecule pull-down (SiMPull) super-resolution microscopy was performed as previously described (*18*). Briefly, passivated PEGylated glass coverslips were coated with 10nM biotinylated Ht7 (Invitrogen, MN1000B) capture antibody diluted in blocking solution (1mg/mL BSA in PBS) for 10 minutes. This was followed by washing in PBST (0.05% Tween-20 in PBS: 50mM tris base, 150 mM NaCl, pH 7.4) and 10 minutes incubation in blocking solution. After another wash in PBST, 10µL of sample (1:50 dilution in PBS) was added and left to incubate for 1 hour at room temperature, followed by washing in TBST. Ht7 labelled with a covalently coupled docking strand (DBCO TEG-AAACCACCACCACCACCACCACCACCACCACCA) was used for detection at 3nM in blocking solution, being incubated on the slide for 15 minutes, followed by a

final wash in PBS. 3µL imaging strands (1 nM in PBS, TATGTAGATC-AminoC7 - Atto655) were then added before the gasket was sealed with another clean coverslip.

Imaging was done on a home-built total internal reflection fluorescence (TIRF) microscope, consisting of an inverted Ti-2 Eclipse microscope body (Nikon) fitted with a 1.49 N.A., 60x TIRF objective (Apo TIRF, Nikon) and a perfect focus system. Images were acquired using a 638 nm laser (Cobolt 06-MLD-638, HÜBNER). Images were collected in a grid using an automated script (Micro-Manager) to avoid any bias in the selection of FOVs. Images were acquired for 7000 frames of 100 ms exposure. Super-resolution images were reconstructed using the Picasso package. Localizations were identified and fit using IFComDet then corrected for microscope drift using the inbuilt implementation of redundant cross-correlation. Localizations were then filtered for precision <30 nm and then clustered using DBSCAN as provided by the scitkit-learn package with permissive parameters (radius of 0.25 and minimum density of 5). The skeletonized length of each aggregate was measured whereby the length of each aggregate is reported as the summed branch distance. Finally, super-resolved images were rendered using the inbuilt Picasso functionality.

Mass Spectrometry

For mass spectrometry analysis, 50ug of each cell lysate sample was diluted to 1µg/µL using 25mM AMBIC. Cysteines were reduced by adding DTT to a final concentration of 4mM and heating the samples to 60°C for a total of 10 minutes. To prevent cysteine re-oxidation iodoacetamide was added as an alkylating reagent to a final concentration of 14mM and incubation proceeded for 45 minutes at room temperature in the dark. Digestion was carried out semi-automatically on a Kingfisher Apex using the Protein Aggregation Capture method adapted from (*32*). Briefly, reduced and alkylated samples were transferred to a 96 well plate and precipitated by adding acetonitrile to a final concentration of 70% (v/v). Washed MagResyn Hydroxyl microparticles from Resyn Biosciences were immediately to the samples at a ratio of 1:4 (protein:bead) to promote protein precipitation and on-bead aggregation. Three subsequent washes of the beads with the aggregated proteins was performed with 100% acetonitrile and followed by two additional washes with 70% ethanol. In-bead digestion was performed on a first stage on the Kingfisher Apex by adding 1µg of trypsin to 100uL of 25mM AMBIC containing 0.2% (v/v) RapiGest detergent (Waters) and incubating for 1h at 47°C. Overnight digestion was then carried out at 37°C on an Eppendorf ThermoMixer C for an additional 16h. Magnetic beads were removed and peptides were acidified with the addition of trifluoroacetic acid to a final concentration of 0.5% (v/v). The acidified tryptic digest was then centrifuged at 13,000 x *g* for 15 minutes to remove RapiGest degradation by-products and the supernatant subjected to LC-MS/MS analysis.

LC-MS/MS was performed on an Vanquish Neo UHPLC (ThermoFisher Scientific, San Jose, USA) hyphenated to an Orbitrap Eclipse mass spectrometer (ThermoFisher Scientific, San Jose, USA). Peptides were trapped on a C18 Acclaim PepMap 100 (5 µm, 300 µm x 5mm) trap column (ThermoFisher Scientific, San Jose, USA) and separated on a C18 Aurora Ultimate TS (25cm x 75 µm) column (IonOpticks, Australia) over a gradient of solvent B [80 % (v/v) acetonitrile, 0.1% formic acid] from 3% to 25% B over 135 minutes followed by a 25% to 45 %B over 45minutes. MS1 full scans were acquired in the Orbitrap at a resolution of 120,000 (AGC target of 4e5 ions

with a maximum injection time of 50ms) and followed by MS2 in a data-independent acquisition setting composed of 41 staggered variable width window covering 400-900 m/z. MS2 DIA scans were acquired in the Orbitrap at a resolution of 30,000 with a maximum injection time of 54ms and an HCD collision energy of 30%.

Raw data were imported and processed in Spectronaut 18.0 (Biognosys) using stringent criteria as set out in (*33*). Raw files were searched against *Homo sapiens* protein sequences downloaded from UniProt (UP000005640_9606) with the overexpressed proteins appended to the protein database (TauP301S-Venus; R-NbF8-2 and mCherry). Differential abundance testing was performed using unpaired t-test with group-wise testing correction.

AAV preparation

Chimeric particles of adeno-associated virus produced with capsids of types 1 and 2 (AAV1/2) were prepared as previously describe (*34*). 7µg pAAV-hSyn/CAG-Transgene, 3.5µg pAAV2/1 Rep-Cap, 3.5µg pAAV2/2 Rep-Cap and 20µg pAdDeltaF6 helper plasmid per plate were co-transfected in 10×15 cm cell culture dishes of 60% confluent AAVpro® HEK293T cells (Takara, 632273) via polyethylenimine (PEI). After 60 hours, medium was collected and cells resuspended in 10 mL total AAV lysis buffer (20mM Tris pH 8.0, 1mM $MgCl_2$, 150mM NaCl). NaCl (0.93 g) and 10mL of 40% polyethylene glycol 8000 (PEG) was added per 40mL media and incubated on ice overnight, after which AAV was precipitated via centrifugation and resuspended in 4 mL total AAV lysis buffer and pooled with the cell pellet. Combined resuspended pellets were incubated with 1mM $MgCl_2$ and 100U benzonase for 15 mins at 37°C and then freeze-thawed 3 times before a final benzonase digestion with an additional 100U. This suspension was then centrifuged, with AAV containing supernatants being collected and then subjected to iodixanol (Optiprep) (Sigma-Aldrich, D1556) gradient ultracentrifugation. Iodixanol was layered into a 38.5mL ultracentrifuge tube (Beckman, 344326) with the following solutions: 6mL of 17% (5mL 10x PBS, 0.05mL 1M $MgCl_2$, 0.125mL 1M KCl, 10mL 5M NaCl, 12.5mL Optiprep, H_2O to 50mL), 6mL of 25% (5mL 10x PBS, 0.05mL 1M $MgCl_2$, 0.125mL 1M KCl, 20mL Optiprep, 0.1mL of 0.5% phenol red, H_2O to 50mL), 5mL of 40% (5mL 10x PBS, 0.05mL 1M $MgCl_2$, 0.125mL 1M KCl, 33.3mL Optiprep and H_2O to 50mL) and 6mL of 60% (0.05mL 1M $MgCl_2$, 0.125mL 1M KCI, 50mL Optiprep, 0.025mL 0.5% phenol red). AAV containing supernatants were then layered on top of the 17% layer and ultracentrifuged (68,000 RPM, 17°C, 70 mins) in a Type 70Ti rotor (Beckman, 337922). The 40% iodixanol fraction was isolated and concentrated to ~100 µL in PBS, with single use aliquots being frozen at −80°C. AAV titers were determined via SYBR® Green qPCR (ThermoFisher, 4344463) according to the manufacturers protocol using forward (GGAACCCCTAGTGATGGAGTT) and reverse (CGGCCTCAGTGAGCGA) primers for the AAV ITR regions. AAV purity was determined via SDS-PAGE followed by Coomassie staining. AAV_{9P31} was prepared following the same protocol, but replacing the AAV2/1 and AAV2/2 Rep-Cap plasmids with an AAV9 Rep-Cap with a WPTSYDA heptapeptide inserted between residues 558 and 589 of the VP1 gene via site directed mutagenesis (*24*).

Mice and AAV injections

All animal work was licensed under the UK Animals (Scientific Procedures) Act 1986 and was approved by the Medical Research Council Animal Welfare and Ethical Review Body. H2B-GFP transgenic mice (CAG:H2B-EGFP) were obtained from Jackson Laboratory (MGI:3686857). Tg2541 transgenic mice (MGI:3778191), which express human 0N4R P301S tau under the control of a Thy1 promoter (*16*), were obtained from Dr Michel Goedert, MRC Laboratory of Molecular Biology, UK. A spread of litters and sexes were used for all primary culture and in vivo experiments. Power analysis for in vivo group sizes was performed using pilot data with alpha = 0.05; beta = 0.8.

Stereotaxic injection of $2x10^9$ genome copies (GC) AAV1/2 into the left hippocampus of 2-month-old H2B-GFP transgenic mice was performed using coordinates: AP: -1.60, ML: +1.36, DV: −1.2mm. Two injections of $2x10^9$ GC were administered to the left frontal cortex of 5.5-month-old Tg2541 tau transgenic mice at the coordinates: AP: +2.96, ML: +0.75, DV: -0.75 mm; and AP: +2.46, ML: +1.64, DV: -1.13 mm. $1x10^{11}$ GC AAV-9P31 was injected intravenously through the tail vein of 4- or 5.5-month-old Tg2541 tau transgenic mice. All injections were performed under anesthetic using isoflurane inhalation (induction = 2% isoflurane 1L/minute O2, maintain = 1% isoflurane 1L/minute O2).

For performing histological analysis, mice were culled by exsanguination and perfused with pre-cooled 4% PFA. Brain and spinal cord samples were collected in PFA overnight, dehydrated in 30% sucrose in PBS (w/v) and then stored at -80°C until slicing into 30µm sections on a cryostat. For immunoblot analysis, mice were culled by exsanguination with samples were collected in pre-cooled PBS and then stored at -80°C.

GFP ELISA

Injected and non-injected H2B-GFP mouse hippocampi were isolated and separately homogenised as described above. H2B-GFP protein levels in these homogenates were quantified using a GFP ELISA kit (Abcam, ab171581) as per the manufacturer's instructions.

Fluorescent microscopy and immunofluorescence of mouse brain sections

Brain/Spinal cord slices were mounted onto Superfrost Plus (ThermoFisher, 10149870) glass slides. For IF staining, mounted slices were blocked and permeabilised for one hour using PBS containing 10% goat serum and 0.3% Triton X-100, followed by incubation with primary antibodies in antibody diluent (PBS containing 1% goat serum and 0.003% Triton X-100) overnight at 4°C on a shaking incubator in the dark. Biotin conjugated mouse AT8 (Invitrogen, MN1020B) was used at 1:1200, with the rabbit Dako anti-total tau antibody (Dako, A0024) being used at 1:1000. Following this overnight incubation, primary antibodies were removed, and slides washed in PBS. Streptavidin conjugated Alexa Fluor 647 (Invitrogen, S32357) (1:500) and goat anti-rabbit Alexa Fluor 647 (Invitrogen, A21245) were then incubated with slides in antibody diluent for 2 hours at room temperature, after which secondary antibodies were removed and slides washed again in PBS. Hoechst 33342 (1µg/ml in PBS) was then added at for 5-10 minutes to stain

nuclei, followed by a final wash in PBS. Coverslips were then added to slides, and images acquired the next day using an Eclipse Ti2 microscope, with AT8/GFP coverage being quantified in ImageJ.

Primary mouse neuron cultures

Brains were removed from the heads of P0 or P1 mice and pooled cortex and hippocampal neuronal cultures were prepared as previously described (*35*, *36*). Hippocampi and cortices were dissected in ice cold Hibernate-A (Gibco, A1247501) and the meninges removed. Tissues were pooled in a 15mL conical tube and washed twice with room temperature Hibernate-A before being incubated with a final concentration of 0.25% trypsin (Gibco, 15090-046), at 37°C for 20 minutes. During this period, a cotton-plugged glass Pasteur pipette (Merck Life Science, S6143) was fire-polished. Following trypsinisation, 500µL 1% (w/v) DNAse I (Sigma-Aldrich, DN25) was added to the tissue and incubated at room temperature for 5 minutes. The tissue was washed twice with 37°C Hibernate-A, followed by two washes with 37°C neuron plating medium (PM) containing Neurobasal Plus (Gibco, A3582901), 1 mM GlutaMAX (Gibco, 15050061), 1% penicillin-streptomycin (Invitrogen, 15140122), 10 % horse serum (Invitrogen, 26050070), and 1x B-27 Plus supplement (Gibco, A352801). After washing, 2.5 ml PM was added to the tissue, and the tissue was triturated using the glass pipette in a 60 mm dish. A further 8 mL of PM was added to the dish, and the cell suspension passed through a 70 µm cell strainer. Live cells were counted via trypan blue staining using the Countess II automated cell counter (Invitrogen). For tau seeding experiments, 30,000 cells/well were seeded into black 96-well plates (Greiner Bio-One, 655090), coated with poly-L-lysine (RnD Systems, 3438-100-01). After 4 h, all media was removed and replaced with maintenance media (MM) (PM without serum). All primary cultures were maintained in a humidified tissue culture incubator at 37 °C with 5 % CO2.

Quantification of seeded tau aggregation in primary mouse neurons

Seeded tau aggregation was induced in primary mouse neurons via the addition of 50nM recombinantly produced 0N4R P301S-tau assemblies in maintenance media and quantified via IF. Media was removed from neurons followed by two washes with ice cold PBS, after which neurons were fixed and permeabilised via the addition of 100µL/well ice cold methanol for 3 minutes on ice. Following this incubation, 100µL PBS was added to dilute the methanol, and then 100µL of this mixture was removed. This dilution step was repeated a total of three times, after which all liquid was removed from the well. Fixed neurons were then washed with PBS and blocked with 2% BSA in PBS (Neuron IF block) for 30 minutes at room temperature.

Primary antibody solutions were made up in neuron IF block at the following concentrations: Rabbit anti-phospho-tau serine 422 (pS422) (Abcam, ab79415) 1:1000; Chicken anti-MAP2 (Abcam, ab5392) 1:5000; Mouse anti-phospho-tau serine 202 and threonine 205 (AT8) (Invitrogen, MN1020) 1:1000. Neurons were incubated with primary antibody overnight at 4°C. The following day, primary antibody was aspirated, and cells washed with PBS. Secondary antibody solutions were made up in neuron IF block at the following concentrations: goat anti-rabbit Alexa Fluor 647 (Invitrogen, A21245) 1:500; goat anti-chicken Alexa Fluor 488 (Invitrogen, A11039) 1:500; goat anti-mouse Alexa Fluor 647 (Invitrogen, A32728) 1:500; goat anti-chicken Alexa Fluor 568 (Invitrogen, A11041) 1:500. Neurons were incubated with secondary antibody

for 1 hour at room temperature in the dark, after which antibody was removed and neurons were washed with PBS. Finally, 2µg/ml Hoechst 33342 (diluted in PBS) was added to neurons for 10 minutes at room temperature (in the dark), followed by a final wash step in PBS. Cells were left in PBS for fluorescence imaging using an Eclipse Ti2 Microscope. NIS-Elements software (Nikon) was used to quantify pS422 puncta (puncta detection), pS422 cell bodies (thresholding) and MAP2 coverage in each image. Tau seeded primary neurons treated with AAV1/2-hSyn-0N4R P301S tau-venus and AAV1/2-hSyn-R-Nb$_{F8\text{-}2}$-T2A-mCherry were live imaged in an IncuCyte® S3 Live-Cell Analysis System.

HEK Cell Immunofluorescence (IF)

TVA HEK cells cultured in 96-well plates were prepared for immunofluorescence (IF) via methanol fixation and permeabilisation as described above. Fixed HEKs were blocked for 30 minutes at room temperature in HEK IF block (1x TBS containing 5% goat serum, 0.2x fish gelatin, 0.3% Triton X-100 and 0.01% sodium azide), after which they were incubated overnight at 4°C in primary antibody solutions made up in HEK IF block at the following concentrations: Mouse anti-2A peptide (MABS2005, Merck) 1:1000; Rabbit SP70 anti-tau (MA5-16404) 1:1000.

The following day, primary antibody was aspirated, and cells washed with PBS. Secondary antibody solutions were made up in HEK IF block at the following concentrations: goat anti-mouse Alexa Fluor 647 (Invitrogen, A32728) 1:500; goat anti-rabbit Alexa Fluor 568 (Invitrogen, A11011) 1:500. HEKs were incubated with secondary antibody for 1 hour at room temperature in the dark, after which antibody was removed and neurons were washed with PBS. Cells were left in PBS for fluorescence imaging using an Eclipse Ti2 Microscope.

Molecular characterization of tau/H3-2 and tau/ F8-2$_{S54L+T127A}$ interactions

Production and purification of the recombinant tau 2N4R and Nb H3-2 and F8-2 $_{S54L+T127A}$ and NMR analysis of tau-H3-2 complex have been performed according to (*15*). Affinity measurements were performed on a BIAcore T200 optical biosensor instrument (Cytiva), according to (*15*). Briefly, biotinylated-tau was injected on a streptavidin SA sensorchip in HBS-EP + buffer (Cytiva), at a flow-rate of 30 µL/min, until the total amount of captured tau reached 500 resonance units (RUs). Nb H3-2 and F8-2$_{S54L+T127A}$ was injected sequentially with increasing concentrations ranging between 0.125 and 2 mM in a single cycle, with regeneration (three successive washes of 1M NaCl). Single-Cycle Kinetics (SCK) analysis was performed to determine association k_{on} and dissociation k_{off} rate constants by curve fitting of the sensorgrams using the 1:1 Langmuir model of interaction of the BIAevaluation software 2.0 (Cytiva). Dissociation equilibrium constants (K_D) were calculated as k_{off}/k_{on}.

Quantification of tau-venus degradation in TVA/TVS cells following AAV1/2 transduction

20,000 TVA or TVS cells were plated per well of a 96-well plate in FBS free DMEM and transduced with 100,000vg/cell AAV1/2 encoding either R-Nb$_{vhhGFP4}$ or TRIM21 RING or

vhhGFP4 only controls. Cells were longitudinally imaged in situ in an Incucyte S3 system (Sartorius), with images being acquired once every hour.

Validation of VCP inhibition via NMS-873

HEK293 cells were plated in a 24-well plate at 100,000 cells/well. After 24 hours, media was changed to complete DMEM plus 5µM small molecule inhibitor of VCP, NMS-873 or DMSO control. AdV5-GFP was mixed with hIgG1 9C12 antibody with a final concentration of 20ng/ml for 1 hour at RT to allow complex formation. Following 2 hours of pretreatment with drugs or DMSO, 20µl of virus:antibody complexes were added per 500 µl of DMEM per well and incubated for 6 hours at 37ºC, before full media change with complete DMEM. The following day after infection, cells were collected by trypsinisation and GFP infection was analysed via flow cytometry using a Cytoflex (Beckman Coulter) machine. Fold neutralisation was calculated by dividing % infection virus only by % infection with respective antibody concentration.

Diagram Creation

Diagrams presented in figures 1A-D were created with Biorender.com

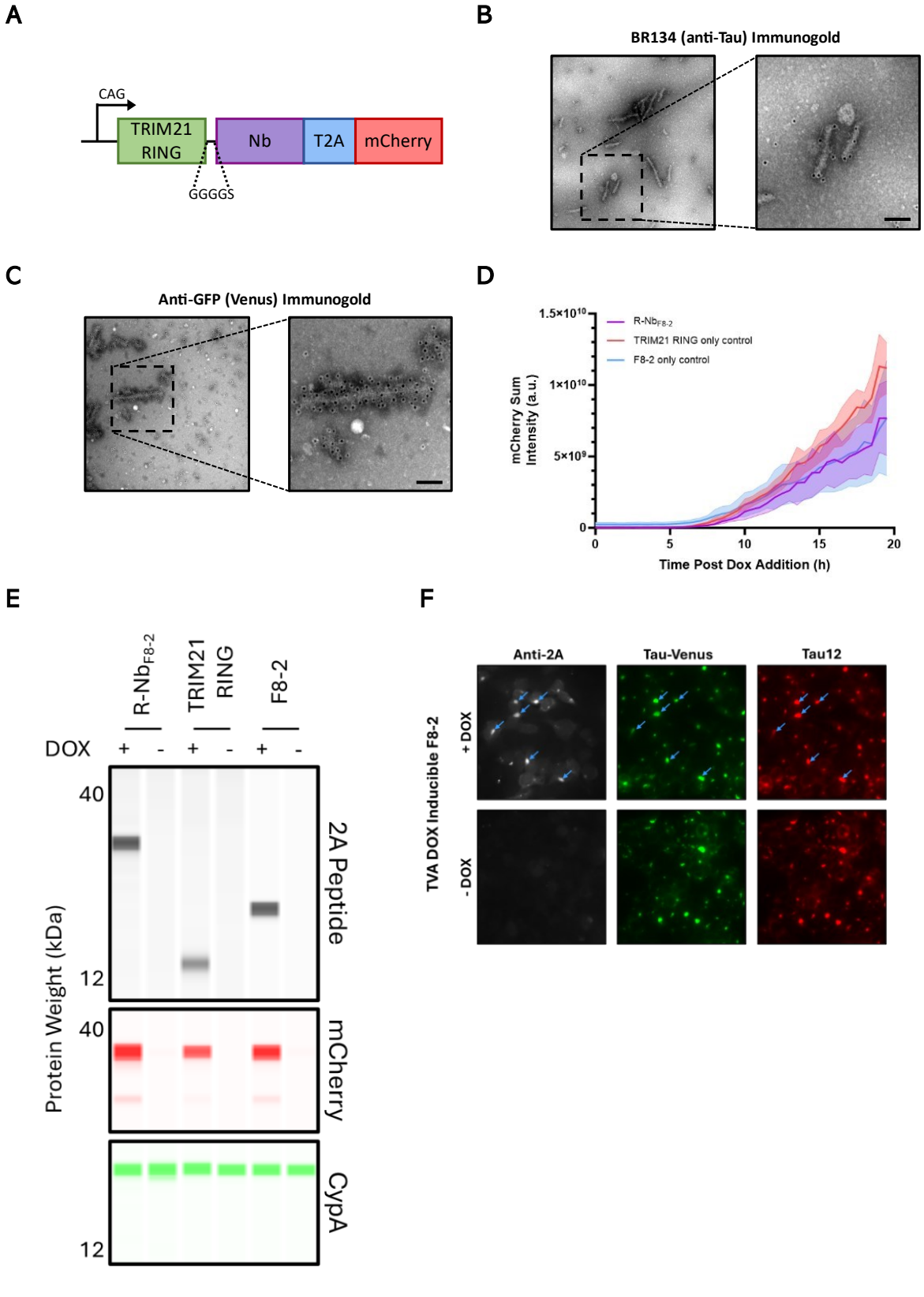
A
CAG
TRIM21 RING
Nb
T2A
mCherry
GGGGS
B
BR134 (anti-Tau) Immunogold
C
Anti-GFP (Venus) Immunogold
D
R-Nb$_{F8-2}$
TRIM21 RING only control
F8-2 only control
mCherry Sum Intensity (a.u.)
1.5×10^{10}
1×10^{10}
5×10^{9}
0
0
5
10
15
20
Time Post Dox Addition (h)
E
R-Nb$_{F8-2}$
TRIM21 RING
F8-2
DOX
+ - + - + -
Protein Weight (kDa)
40
12
2A Peptide
40
mCherry
12
CypA
F
Anti-2A
Tau-Venus
Tau12
TVA DOX Inducible F8-2
+ DOX
- DOX

Fig. S1. R-Nb design, TVA fibril characterisation, and DOX inducible expression of constructs in TVA cells.

(**A**) Schematic of R-Nb constructs consisting of an N-terminal TRIM21 RING domain (residues 1-85) fused to a nanobody via a flexible GGGGS linker. A self-cleaving T2A-mCherry fluorescent tag was included downstream of the R-Nb construct, with expression being driven by the ubiquitous CAG promoter. (**B**) Immunogold electron microscopy images labelling fibrillar aggregates extracted from TVA cells with the BR134 anti-tau antibody, or (**C**) an anti-GFP antibody. Scale bars, 100nm. (**D**) Sum mCherry intensity from TVA cells expressing either DOX inducible R-Nb_{F8-2}, TRIM21 RING or F8-2, following DOX addition. (**E**) Immunoblot of lysates from the same TVA cells +/- DOX addition for 15 hours, probing for mCherry, CypA (loading control) and the N-terminal product (either R-Nb_{F8-2}, TRIM21 RING, or F8-2) via an anti-2A peptide antibody. (**F**) IF images from TVA cells expressing DOX inducible F8-2 nanobody (15 hours post DOX addition) demonstrating colocalisation (blue arrows) of F8-2 (2A antibody signal) with aggregated tau venus and Tau12 antibody staining. Shaded areas represent mean ± SD. (D) n = 8 biological replicates per condition.

A

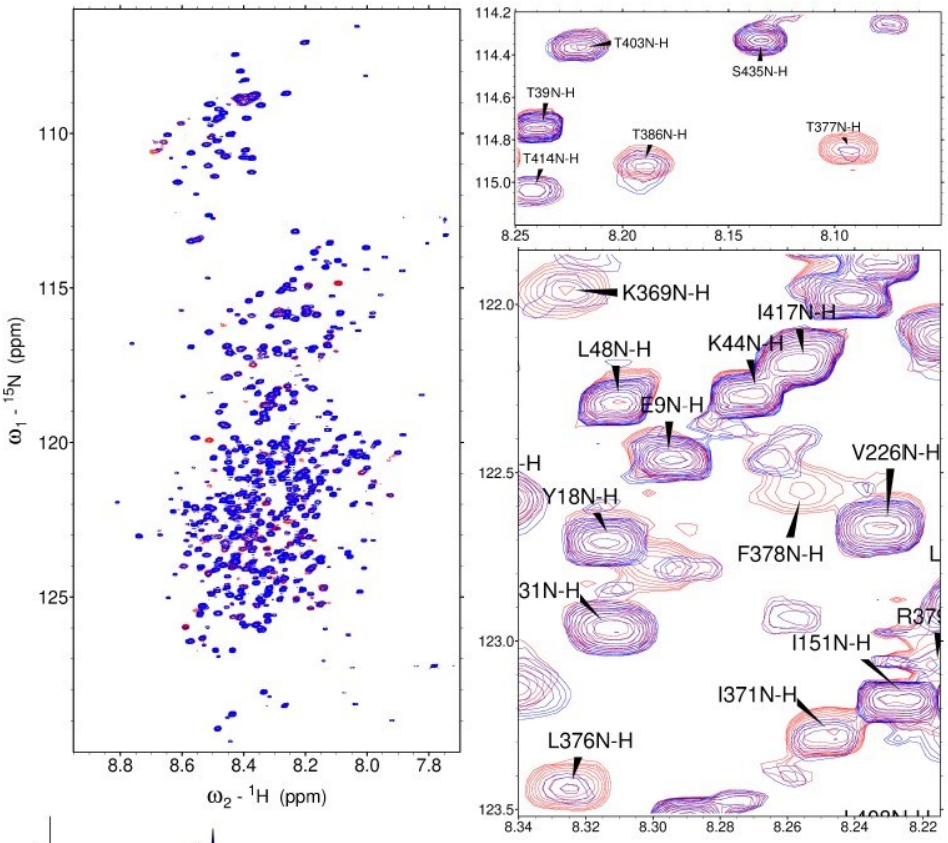

B

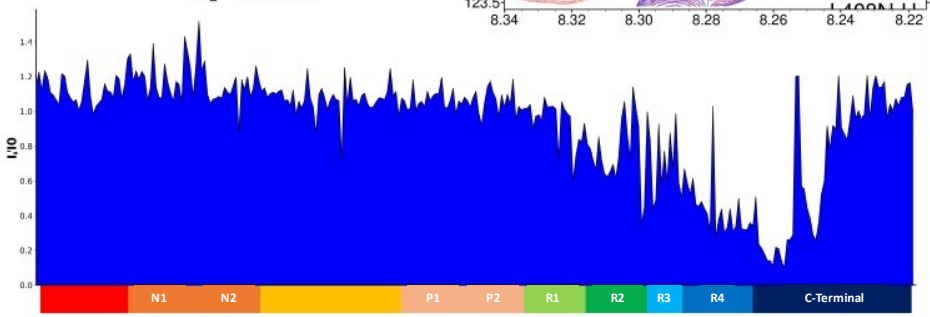

C

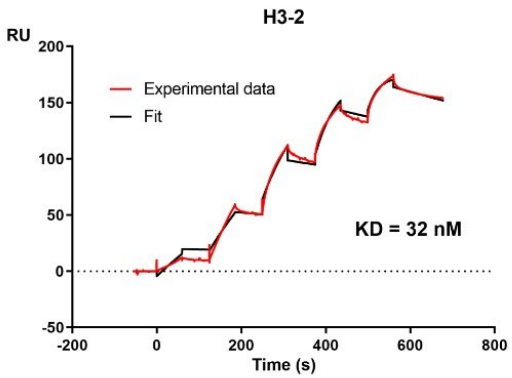

VHH	k_{on} ($M^{-1}.s^{-1}$)*10^{+2}	k_{off} (s^{-1})*10^{-3}	KD (nM)
H3-2	207 ± 2,1	0,7 ± 0,02	32 ± 1,2

D

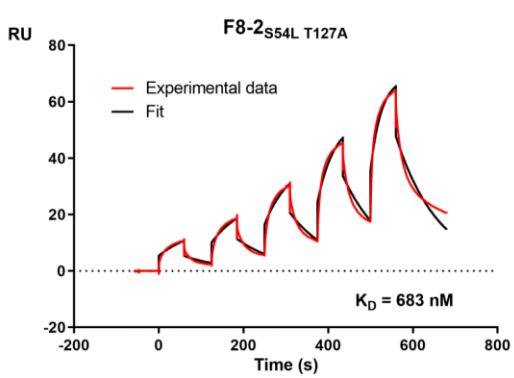

VHH	k_{on} ($M^{-1}.s^{-1}$)*10^{+2}	k_{off} (s^{-1})*10^{-3}	KD (nM)
F8-$2_{S54L\ T127A}$	143,7 ± 1,47	9,8 ± 0,05	683 ± 8

Fig. S2. Determination of H3-2 nanobody epitope and H3-2/F8-2$_{S54L+T127A}$ affinities.

(**A**) Overlay of ^{1}H, ^{15}N HSQC two-dimensional spectra and enlargements of free 2N4R tau (in red) or 2N4R tau mixed at equimolar ratio with non-labeled H3-2 nanobody (superimposed in blue) (n = 1). In the spectrum of tau in the presence of H3-2, multiple resonances are broadened beyond detection compared with the tau control spectrum. (**B**) Normalized NMR intensities (I/I0) along the tau sequence with (I0) and (I) corresponding to the resonance intensity when tau is free in solution or mixed with equimolar quantity of H3-2 (I), respectively. The normalized intensity ratios (I/I0) plot allowed the identification of the tau C-terminus domain as the target of H3-2 interaction. N1 and N2 are two alternatively-spliced regions in the N-terminal domain (1–163), the proline-rich domain is subdivided in P1 and P2 regions, the MTBD consists of four partially repeated regions, R1 to R4. (**C**) Sensorgrams (reference subtracted data) of single cycle kinetics analysis performed on immobilized biotinylated tau, with five injections of H3-2 or (**D**) F8-2$_{S54L+T127A}$ at 0.125 µM, 0.25 µM, 0.5 µM, 1 µM, and 2 µM (n = 1). Dissociation equilibrium constant (K_D) was calculated from the ratio of off-rate and on-rate kinetic constants k_{off}/k_{on}. K_{on} and k_{off} values are included in the table. Black lines correspond to the fitted curves, red lines to the measurements.

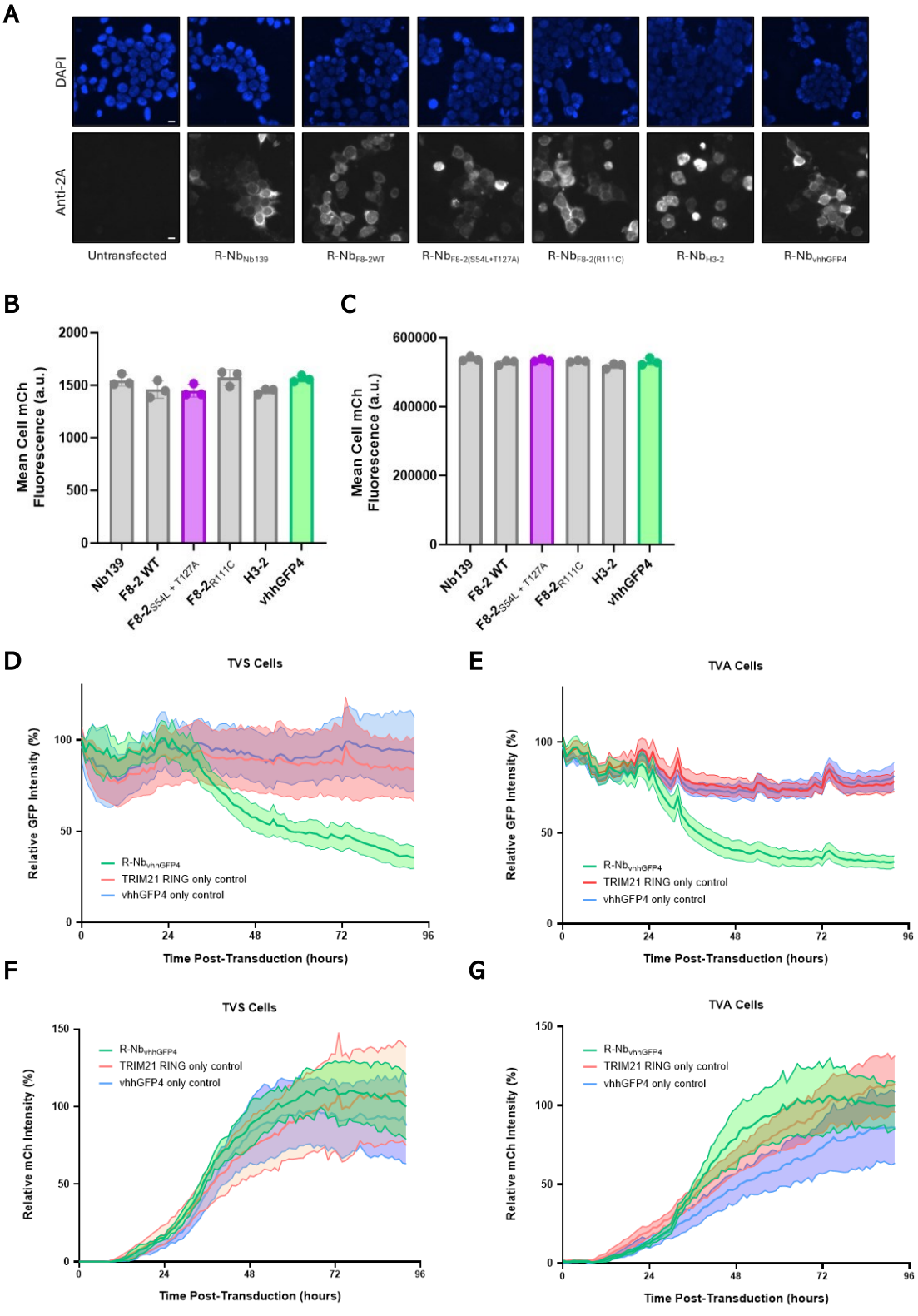
A
DAPI
Anti-2A
Untransfected
R-Nb$_{Nb139}$
R-Nb$_{F8-2WT}$
R-Nb$_{F8-2(S54L+T127A)}$
R-Nb$_{F8-2(R111C)}$
R-Nb$_{H3-2}$
R-Nb$_{vhhGFP4}$
B
Mean Cell mCh Fluorescence (a.u.)
2000
1500
1000
500
0
Nb139
F8-2 WT
F8-2$_{S54L + T127A}$
F8-2$_{R111C}$
H3-2
vhhGFP4
C
Mean Cell mCh Fluorescence (a.u.)
600000
400000
200000
0
Nb139
F8-2 WT
F8-2$_{S54L + T127A}$
F8-2$_{R111C}$
H3-2
vhhGFP4
D
TVS Cells
Relative GFP Intensity (%)
100
50
0
R-Nb$_{vhhGFP4}$
TRIM21 RING only control
vhhGFP4 only control
0
24
48
72
96
Time Post-Transduction (hours)
E
TVA Cells
Relative GFP Intensity (%)
100
50
0
R-Nb$_{vhhGFP4}$
TRIM21 RING only control
vhhGFP4 only control
0
24
48
72
96
Time Post-Transduction (hours)
F
TVS Cells
Relative mCh Intensity (%)
150
100
50
0
R-Nb$_{vhhGFP4}$
TRIM21 RING only control
vhhGFP4 only control
0
24
48
72
96
Time Post-Transduction (hours)
G
TVA Cells
Relative mCh Intensity (%)
150
100
50
0
R-Nb$_{vhhGFP4}$
TRIM21 RING only control
vhhGFP4 only control
0
24
48
72
96
Time Post-Transduction (hours)

5

Fig. S3. Expression of R-Nb constructs in HEK293, TVA and TVS cells, and tau-venus degradation kinetics.

(**A**) Representative IF images from HEK293 cells transfected with R-Nb constructs, stained for R-Nb protein via an anti-2A antibody and for nuclei with DAPI. (**B**) R-Nb expression in transfected and analysed TVA and (**C**) TVS cells, quantified by either fluorescent microscopy or flow cytometry respectively as mean cell mCherry fluorescence. (**D**) GFP intensity (normalised to cell count and plotted as % signal compared to zero-hour timepoint) of TVS cells or (**E**) TVA cells (GFP intensity normalised against confluence and plotted as % signal compared to zero-hour timepoint), over time following transduction with AAV1/2 encoding either R-Nb$_{vhhGFP4}$ or TRIM21 RING or vhhGFP4 only controls. (**F**) mCherry positive cell count (normalised to total cell count and plotted as % signal compared to zero-hour timepoint) from TVS cells or (**G**) TVA cells (mCherry positive cell count normalised against confluence and plotted as % signal compared to zero-hour timepoint), over time following transduction with AAV1/2 encoding either R-Nb$_{vhhGFP4}$ or TRIM21 RING or vhhGFP4 only controls. Shaded areas represent mean ± SD. (B) and (C) n = 3 biological repeats per condition. (D-G) n = 5 technical replicates per condition.

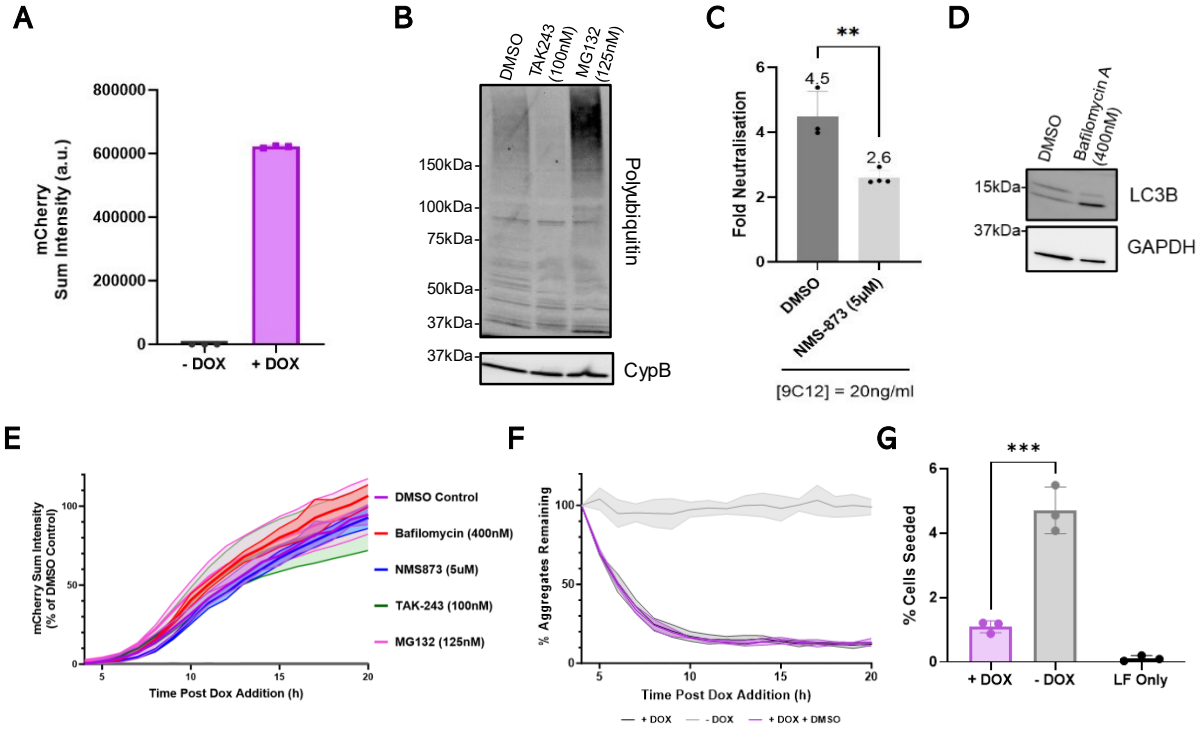
A
mCherry Sum Intensity (a.u.)
800000
600000
400000
200000
0
- DOX
+ DOX
B
DMSO
TAK243 (100nM)
MG132 (125nM)
150kDa
100kDa
75kDa
50kDa
37kDa
37kDa
Polyubiquitin
CypB
C
**
Fold Neutralisation
6
4
2
0
4.5
2.6
DMSO
NMS-873 (5μM)
[9C12] = 20ng/ml
D
DMSO
Bafilomycin A (400nM)
15kDa
37kDa
LC3B
GAPDH
E
mCherry Sum Intensity (% of DMSO Control)
100
50
0
5
10
15
20
Time Post Dox Addition (h)
DMSO Control
Bafilomycin (400nM)
NMS873 (5uM)
TAK-243 (100nM)
MG132 (125nM)
F
% Aggregates Remaining
100
50
0
5
10
15
20
Time Post Dox Addition (h)
+ DOX
- DOX
+ DOX + DMSO
G
***
% Cells Seeded
6
4
2
0
+ DOX
- DOX
LF Only

Fig. S4. Expression of R-Nb in TVS Cells, Validation and Effects of Pharmacological Inhibition on R-Nb Expression, and Supernatant Secondary Seeding

(**A**) Integrated mCherry intensity from TVS cells expressing DOX inducible R-Nb_{F8-2} 24 hours after treatment with, or without, DOX, quantified via fluorescent microscopy. (**B**) Western blot of TVA cells treated with DOX and DMSO (solvent control), TAK243 (E1 inhibitor) or MG132 (proteasome inhibitor) for 10 hours. Samples were blotted for ubiquitin to validate inhibitor function, and for CypB as a loading control. (**C**) VCP is essential for antibody/TRIM21 mediated virus neutralization (*12*). The ability of NMS-873 to inhibit VCP was therefore assessed via a viral neutralization assay in which adenovirus encoding GFP was neutralised by the anti-adenovirus antibody 9C12. (**D**) Western blot of TVA cells treated with DOX and DMSO or Bafilomycin A for 10 hours, probed for increased LC3B to confirm autophagy inhibition, and GAPDH as a loading control. (**E**) Sum mCherry intensity from DOX inducible R-Nb_{F8-2} TVA cells following addition of DOX and various small molecule inhibitors, quantified via fluorescent microscopy. (**F**) Quantification of tau-venus aggregates from live cell imaging of TVA cells expressing DOX inducible R-Nb_{F8-2} treated with and without DMSO at the highest concentration used as solvent for small molecule inhibitors (0.5%). Quantified via live cell microscopy. (**G**) Supernatants from TVA cells treated with, or without, DOX for 72 hours to induce expression of R-Nb_{F8-2} were introduced to TVS cells via Lipofectamine. Seeded aggregation of soluble tau-venus was quantified 72 hours later via fluorescent microscopy. TVS cells were treated with lipofectamine (LF) only as a negative control. Error bars and shaded areas represent mean ± SD. (A), (E), (F) and (G) n = 3 biological replicates per condition. (C) n = 4 biological replicates per condition. (C) unpaired *t* test. (G) one-way analysis of variance (ANOVA) with Tukey's correction for multiple comparisons. $^{**}P < 0.01$; $^{***}P < 0.001$.

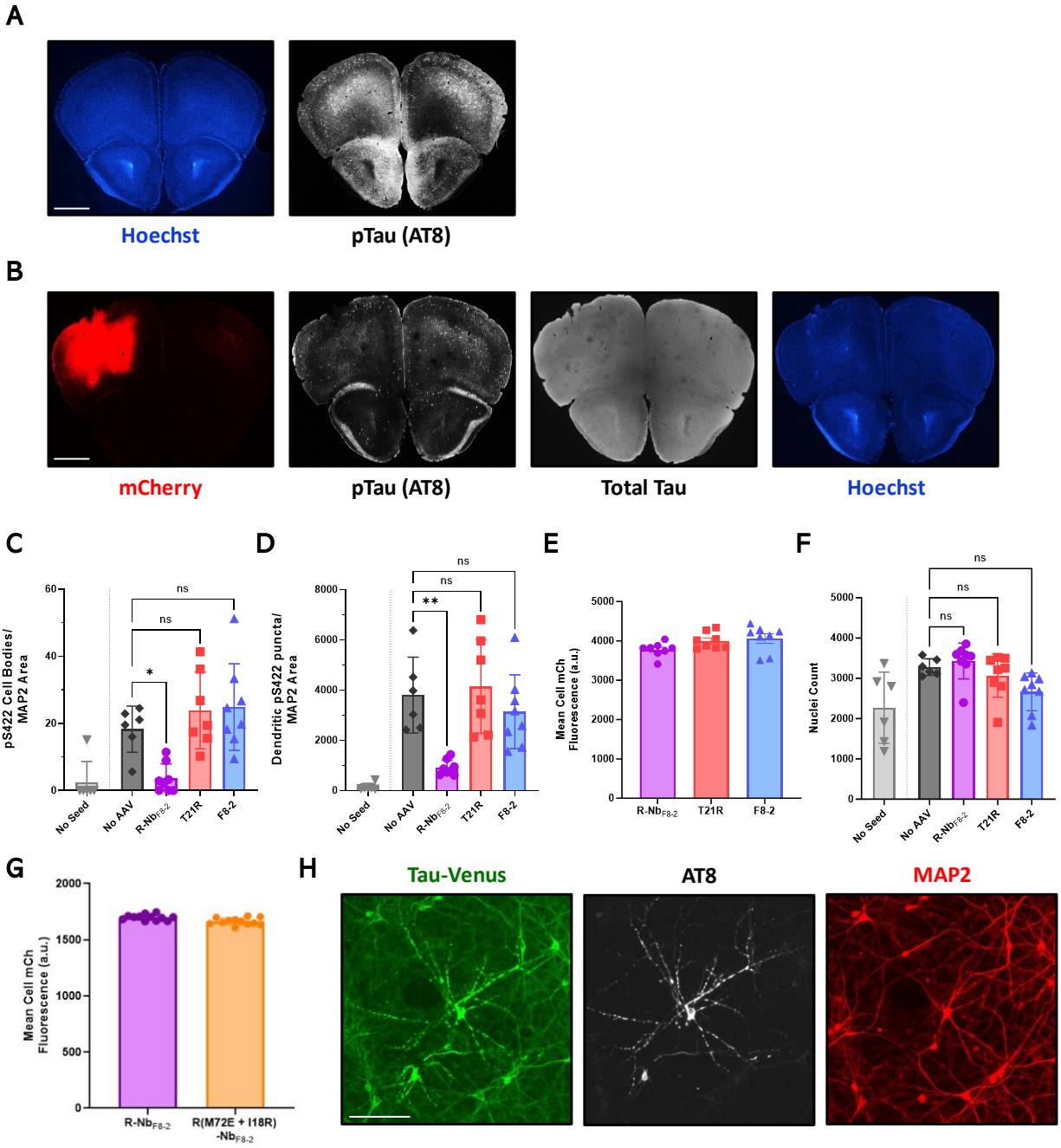
A
Hoechst
pTau (AT8)
B
mCherry
pTau (AT8)
Total Tau
Hoechst
C
pS422 Cell Bodies/ MAP2 Area
No Seed
No AAV
R-NbF8-2
T21R
F8-2
D
Dendritic pS422 puncta/ MAP2 Area
E
Mean Cell mCh Fluorescence (a.u.)
R-NbF8-2
T21R
F8-2
F
Nuclei Count
G
Mean Cell mCh Fluorescence (a.u.)
R-NbF8-2
R(M72E + I18R) -NbF8-2
H
Tau-Venus
AT8
MAP2

5

Fig. S5. Reduction of tau pathology in the aged mouse brain and primary neurons via R-Nb$_{F8-2}$.

(**A**) Representative IF images from frontal cortex of 5.5-month-old Tg2541 mouse. Stained for total nuclei with Hoechst and phosphorylated tau aggregates with AT8. Scale bar, 1mm (**B**) Representative IF images 10 days post-stereotaxic injection of AAV1/2-CAG-R-Nb$_{F8-2}$-T2A-mCherry into the frontal cortex of a 5.5-month-old mouse. Two injections of 2x10^9 GC were used. pTau and total tau were detected using AT8 and DAKO antibodies respectively. Scale bar, 1mm. (**C**) Quantification of pS422 positive cell bodies and (**D**) dendritic puncta normalised against MAP2 coverage from IF images. Seeded neurons were pre-treated with AAV1/2 encoding R-Nb$_{F8-2}$, TRIM21 RING (T21R) or F8-2 only. (**E**) Mean cell mCherry fluorescence of primary neuron cultures treated with AAV1/2-hSyn encoding either R-Nb$_{F8-2}$, TRIM21 RING, or F8-2 with a T2A-mCherry reporter. (**F**) Mean number of nuclei per well of unseeded and tau seeded primary neurons treated with or without the same AAV1/2-hSyn vectors. (**G**) Mean cell mCherry fluorescence of primary neuron cultures treated with AAV1/2-hSyn encoding either active or catalytically dead (M72E+I18R RING mutations) R-Nb$_{F8-2}$ with a T2A-mCherry reporter. (**H**) Representative images from primary neuron cultures prepared from the cortices of neonatal wild-type C57BL/6 mouse pups transduced with AAV1/2-hSyn-0N4R P301S tau-venus (20,000 GC/cell) for 12 days, followed by seeding with heparin assembled P301S tau assemblies for 7 days. Tau-venus was detected with an anti-GFP antibody, with phosphorylated tau aggregates detected using the AT8 antibody and neurons identified via MAP2 staining. Scale bar, 100µm. Error bars represent mean ± SD. (C-F) each point represents the average of two technical repeats from n = 6 to 8 biological repeats. (G) each point represents one of n = 12 biological replicates. (C, D and F) ANOVA with Tukey's correction for multiple comparisons. ns, not significant; *$P < 0.05$; **$P < 0.01$.

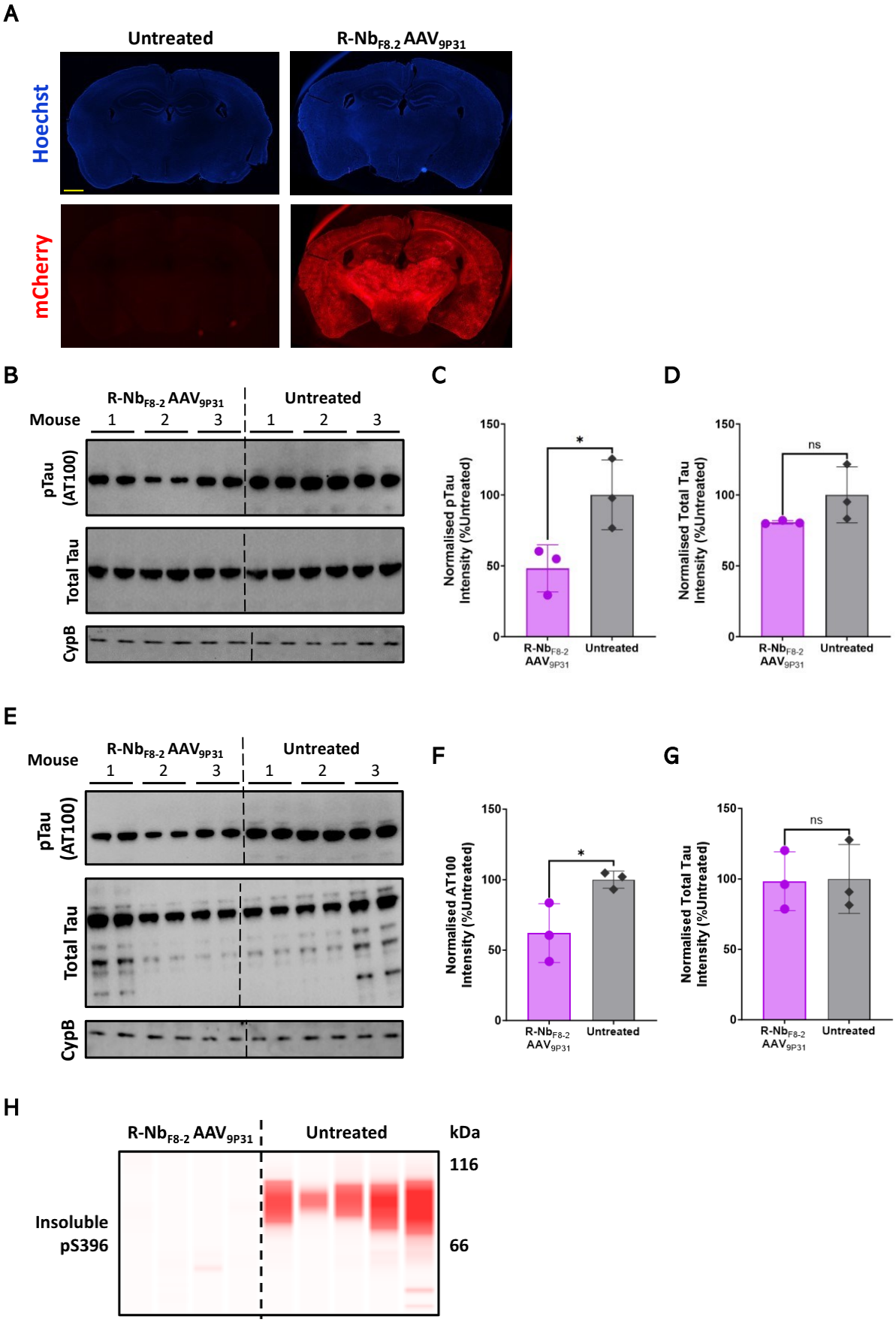
A
Untreated
R-Nb$_{F8.2}$ AAV$_{9P31}$
Hoechst
mCherry
B
R-Nb$_{F8-2}$ AAV$_{9P31}$
Untreated
Mouse
1 2 3 1 2 3
pTau (AT100)
Total Tau
CypB
C
Normalised pTau Intensity (%Untreated)
150
100
50
0
*
R-Nb$_{F8-2}$ AAV$_{9P31}$
Untreated
D
Normalised Total Tau Intensity (%Untreated)
ns
E
F
Normalised AT100 Intensity (%Untreated)
G
Normalised Total Tau Intensity (%Untreated)
H
kDa
116
66
Insoluble pS396

Fig. S6. AAV_{9P31} transduction efficiency and blots from Tg2541 mice treated with AAV_{9P31} R-$Nb_{F8\text{-}2}$ for 10 days or 2 months.

(**A**) Representative fluorescent microscopy images of brain sections from an adult mouse 2 weeks after tail vein injection with $5x10^{11}$ CG of AAV_{9P31} R-$Nb_{F8\text{-}2}$ (with T2A-mCherry reporter). Scale bar, 1mm (**B**) Western blot on whole brain lysates from 5.5-month-old mice treated with $1x10^{11}$ GC AAV_{9P31} R-$Nb_{F8\text{-}2}$ for 10 days, compared to untreated mice. Samples from each mouse were run in duplicate and probed for pTau (AT100), total tau (BR134), and CypB as a loading control. (**C**) Quantification of AT100 pTau and (**D**) total tau (BR134) band intensity in samples from AAV_{9P31} R-$Nb_{F8\text{-}2}$ treated, and untreated mice. (**E**) Spinal cord lysates from the same mice were similarly probed for pTau (AT100) and total tau (BR134), with band intensities quantified in (**F**) and (**G**) respectively. (**H**) Capillary based immunoblot of sarkosyl insoluble fractions from brains of aged mice treated with or without $1x10^{11}$ GC R-$Nb_{F8\text{-}2}$ AAV_{9P31} for two months, probed for pTau phosphorylated on Ser396. Each lane represents an individual mouse. Error bars represent mean ± SD. (C), (D), (F) and (G) each point represents the average intensity of two technical replicates from one mouse, normalised to CypB signal, plotted as percentage intensity compared to untreated mice. n = 3 mice per condition. Unpaired *t* test, ns, not significant; $*P < 0.05$.

Video S1. Live cell fluorescent microscopy of TVA DOX inducible R-Nb$_{F8-2}$ cells.

Images were captured every 20 minutes for 15 hours, beginning 4 hours post-DOX addition. Tau venus aggregates were visualised in the green channel, with the red channel detecting mCherry (R-Nb$_{F8-2}$ expression reporter). Scale bar, 20µm.

Video S2. Live cell fluorescent microscopy of tau seeded WT neurons expressing tau-venus, transduced with R-Nb$_{F8-2}$ AAV1/2.

Images were captured every three hours for 7 days following R-Nb$_{F8-2}$ addition. Tau venus aggregates were visualised in the green channel, with the red channel detecting mCherry (R-Nb$_{F8-2}$ expression reporter). Scale bar, 20µm.